Structural Characterization of Agonist Binding to A_3 Adenosine Receptor through Biomolecular Simulations and Mutagenesis Experiments

Dimitrios Stamatis,[†] Panagiotis Lagarias,[†] Kerry Barkan,[‡] Eleni Vrontaki,[†] Graham Ladds,[‡,*] Antonios Kolocouris[†,*]

[†] Division of Pharmaceutical Chemistry, Department of Pharmacy, School of Health Sciences, National and Kapodistrian University of Athens, Panepistimiopolis-Zografou, 15771 Athens, Greece

[‡] Department of Pharmacology, University of Cambridge, Tennis Court Road, Cambridge, CB2 1PD, UK.

Keywords: A_3 adenosine receptor, agonist, cAMP, IB-MECA, G protein-coupled receptors, MM-GBSA, molecular dynamics, mutant receptor, mutagenesis studies, NECA

1 Abstract

Adenosine A_3 receptor (A_3R), which is activated by adenosine (Ado, (**1**)), is over-expressed in various tumor cells and it is a promising drug target against cancer cell proliferation and other conditions including asthma, rheumatoid arthritis and ischemic injury. Currently there is no experimental structure of A_3R and in this work the orthosteric binding site of A_3R in complex with two agonists, the non-selective 1-(6-amino-9*H*-purin-9-yl)-1-deoxy-*N*-ethyl-β-D-ribofuranuronamide (NECA, (**2**)) and the selective 1-deoxy-1-[6-[[(3-iodophenyl)methyl]amino]-9*H*-purin-9-yl]-*N*-methyl-β-D-ribofuranuronamide (IB-MECA, (**3**)) was studied. Molecular dynamics simulations (MD) of the wild-type (WT) A_3R in complex with NECA (**2**) or IB-MECA (**3**) were performed to identify the residues important for binding in the orthosteric site and several mutagenic studies were conducted to investigate the agonists binding profile. The Molecular Mechanics-Generalized Born Surface Area (MM-GBSA) free energy calculations were able to distinguish mutations that reduce or negate NECA (**2**) or IB-MECA (**3**) activity from those that maintained or increased activity. The calculated ΔG_{eff} values for both IB-MECA and NECA (**2**) displayed good correlations with experimental activities. The combined computational and experimental results suggested that agonist binding and receptor activation is realized through direct interactions with residues of the orthosteric area, such as π-π interactions with F168$^{5.29}$, van der Waals interactions with L246$^{6.51}$ and I268$^{7.39}$, and hydrogen bond interactions with T94$^{3.36}$, N250$^{6.55}$ S271$^{7.42}$ and H272$^{7.43}$. Mutating these residues to alanine negated agonist activity. Alanine mutation of the directly interacting residues W185$^{5.46}$, L264$^{7.35}$ maintained activity for both agonists although mutation of V169$^{5.30}$ increased NECA (**2**) activity but maintained IB-MECA (**3**). The selectivity of IB-MECA (**3**) against A_3R is not only due to direct interactions with the binding area residues, but also due to indirect effects, through residues positioned at the extracellular loop 2, transmembrane domains 5 and 6, as well as deeper in the orthosteric binding area. Indirect interactions including residues L90$^{3.32}$, M177$^{5.38}$ were critical for both agonists binding, M174$^{5.35}$ was important only for NECA (**2**), and I253$^{6.58}$ was unimportant for agonists binding. Moreover, although V169$^{5.30}$ is considered to be a selectivity filter for A_3R binders, when this residue was mutated to glutamic acid, the activity of IB-MECA (**3**) against A_3R increased. The study aimed at highlighting features of the still-unsolved A_3R that are important for IB-MECA (**3**)and NECA (**2**) binding and may be used for the design of effective ligands.

2 Introduction

Ado (**1**) (Figure 1), a naturally occurring purine nucleoside, is the endogenous agonist of adenosine receptors (ARs). ARs are G protein-coupled receptors (GPCRs) comprising four subtypes; A_1, A_{2A}, A_{2B} and A_3. In particular, A_{2A} and A_{2B} subtypes are activated by Ado (**1**) and coupled through G_s resulting in the stimulation of adenylyl cyclase, and therefore, the increase of 3′,5′-cyclic adenosine monophosphate (cAMP) levels. In contrast, A_1 and A_3 subtypes, when activated by Ado (**1**), inhibit adenylyl cyclase and decrease cAMP levels within cells by coupling to the $G_{i/o}$ family of G proteins [1,2]. Some important biochemical and biological activities of Ado (**1**) are the energy transfer in the form of ATP/ADP, signal transduction, and the depressant effect on heart rate and atrioventricular conduction [3]. Ado (**1**) is involved through its ARs in the regulation of various biological functions in different tissues and organ systems, including cardiovascular, liver, renal, respiratory and central nervous system (CNS) (Wilbur and Marchlinski, 1997; Chen et al., 2013). A_3R is a target for a number of inflammatory diseases, including asthma, rheumatoid arthritis and ischemic injury [5]. In addition, evidence is emerging to suggest that the A_3R is over-expressed in various tumor cells compared to normal cells, presenting the possibility that A_3R may be a viable drug target against cancer cell proliferation [6–13].

Optimization of Ado (**1**) has been achieved after structural modifications of the ribose moiety and by substitutions on the adenine ring [14]. However, NECA (**2**) (Figure 1) and analogues are non-selective AR agonists and their side effects include chest pain, flushing, dyspnea and low blood pressure through the activation or inhibition of different AR subtypes [15]. Among the developed agonists (Deninno et al., 2003; Jeong et al., 2003; Volpini et al., 2002; Melman et al., 2008; Tchilibon et al., 2005), IB-MECA (CF101, Piclidenoson, (**3**)) (Figure 1) and its 2-chloro analogue, Cl-IB-MECA, (CF102, Namodenoson) are the most potent, subtype-selective and widely used A_3R agonists that have progressed to advanced clinical trials for inflammation and cancer, respectively [21] [22]. Both compounds [14] inhibit tumor cell growth according to *in vitro* and *in vivo* tumor models [23–25].

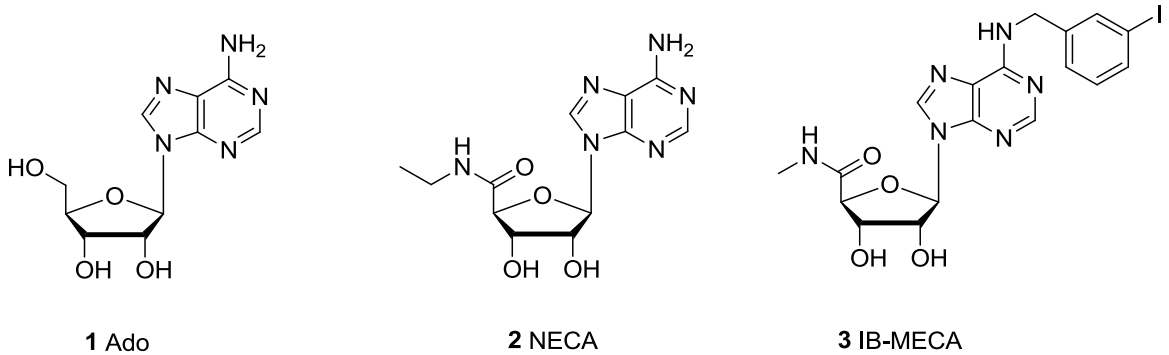

Figure 1. The structures of non-selective AR agonists **1, 2** and of the selective A_3R agonist **3**.

$A_{2A}R$ had been, until recently, the only AR subtype structure that had been determined. The binding mode of agonists like Ado (**1**) and NECA (**2**) [26–28], as well as several antagonists [29–34] inside the $A_{2A}R$ orthosteric binding site has been experimentally revealed using X-ray crystallography or cryo-electron microscopy. In addition, experimental structures of A_1R bound to selective antagonists or Ado (**1**) were resolved using correspondingly X-ray crystallography (Cheng et al., 2017; Glukhova et al., 2017) and cryo-EM [36]. These experimental structures of $A_{2A}R$ and A_1R complexes can be utilized for structure-based drug design. To date, no experimental structure for A_3R has been released, most likely due to difficulties in crystallization, compared to A_1 and A_{2A} receptors, and therefore, homology modeling must be realized to study this receptor in complex with ligands.

Some mutagenesis studies on the A_3R to examine the significance of transmembrane (TM) helical domains TM3, TM5, TM6 and TM7 and second extracellular loop (EL2) to the recognition and binding of NECA (**2**) and other agonists have been performed (Jacobson et al., 2001; Gao et al., 2003, 2002a, 2002b; Duong et al., 2005). These included the mutation of residues $T94^{3.36}$, $H95^{3.37}$, $M177^{5.38}$, $V178^{5.39}$, $N250^{6.55}$, $S271^{7.42}$, $H272^{7.43}$ and $N274^{7.45}$ to alanine, $H272^{7.43}$ to glutamic acid (Jacobson et al., 2001; Gao et al., 2003, 2002a, 2002b), and $Q167^{5.28}$ to alanine, glutamate or arginine (Duong et al., 2005).

The experimental findings from mutagenesis can be combined with computational biochemistry results for the structural mapping of the binding area of a GPCR. A seminal work including a combination of mutagenesis, docking and MD simulations was conducted for A_1R before its experimental structure determination to explore the role of EL2 to agonist binding [40]. Free energy perturbations combined with MD simulations (FEP/MD) have been utilized to investigate accurately how mutations affected ligand selectivity for NECA (**2**)-$A_{2A}R$ complex [41,42] and to optimize purine fragments against $A_{2A}R$ orthosteric binding site [43]. Unbiased long-timescale MD simulations highlighted the role for EL2 in the entry and activation of GPCRs. Interestingly, in those studies, the trajectory of ligands inside the orthosteric pocket involved a metastable state in an extracellular vestibule, delineated by EL2 and EL3, prior to entry into the binding pocket within the helical bundle (Dror et al., 2011; Pan et al., 2013).

Previously we have applied computational drug design to discover potent ligands for ARs. We screened 14,400 compounds from Maybridge HitFinder library against the X-ray structure of $A_{2A}R$ in complex with the selective antagonist ZM241385 [45] using a combination of ligand- and structure-

based approaches. From the 27 compounds selected and tested against all four AR subtypes by radioligand binding assays, most of them were found to be low micromolar A_3R binders and seven were also selective for A_3R [46].

In the present study, we have investigated the orthosteric binding area of A_3R in complex with the non-selective agonist NECA (**2**) and the selective agonist IB-MECA (**3**). We performed MD simulations of the WT A_3R in complex with NECA (**2**) or IB-MECA (**3**) to identify the residues important for binding in the orthosteric binding site. Several mutagenic studies were carried out to study the agonists binding profile. The tested mutations included standard residues of the orthosteric binding area, as well as residues of extracellular loop 2 (EL2) and others that lay in proximity to the bound agonists. These latter residues were studied for their potential role in agonist binding and signal transduction through modulation of the environment that surrounds the ligand inside the binding area. The biological activities of agonists against the mutant proteins were compared with MM-GBSA binding free energy calculations. Compared to the computationally demanding Free Energy Perturbation (FEP)/MD calculations (Keränen et al., 2015), the low-cost MM-GBSA method [47] was applied to investigate the binding of the two agonists against a large number of mutant A_3Rs. The MD simulations and MM-GBSA binding free energy calculations for WT and mutant A_3Rs in complex with **2** or **3** provide insights into important features of the still-unsolved A_3R structure for agonist binding.

3 Computational and Experimental Methods

Models of WT and mutant A_3R - agonist complexes

Adenosine Receptors Models. The NECA (**2**) - active $A_{2A}R$ protein complex (PDB ID 2YDV) [26] was superimposed to WT A_3R ($N12^{1.32}$ - $H304^{7.75}$) which was obtained from the Adenosiland web-service [48]. Superscripted residue numbers refer to the Ballesteros–Weinstein numbering [49]. The WT A_3R receptor model was prepared in Adenosiland web-service through homology modeling, using the PDB ID 2YDV crystal structure of active-state $A_{2A}R$ in complex with NECA (**2**). Then the active $A_{2A}R$ protein conformation was removed resulting in a WT A_3R ($N12^{1.32}$ - $H304^{7.75}$) - NECA (**2**) protein complex model. In the next step, the $A_{2A}R$ in complex with NECA (**2**) and the WT A_3R in complex with NECA (**2**) were optimized using the Protein Preparation Wizard implementation in Schrodinger suite (Protein Prep. Wizard 2015-2; Epik version 2.4, Schrödinger, LLC, New York, NY, 2015; Impact version 5.9, Schrödinger, LLC, New York, NY, 2015; Prime version 3.2,

Schrödinger, LLC, New York, NY, 2015). In this process, the bond orders and disulfide bonds were assigned, and missing hydrogen atoms were added. Additionally, N- and C-termini of the protein model were capped by acetyl and N-methyl-amino groups, respectively. The proteins were subjected in an all atom minimization using the OPLS2005 force field [51] with heavy atom RMSD values constrained to 0.30 Å. The side chain of V169$^{5.30}$ in the WT A_3R - NECA (**2**) complex was rotated to fit the conformer suggested by Katritch *et al.*, in order to increase the free space for the accommodation of agonists with bulky purine 6-NH_2 substitutions [52]. The WT A_3R - NECA (**2**) complex was used for the preparation of the 18 mutant A_3R - NECA (**2**) complexes. The residues investigated computationally for their importance to agonist binding are located in the lower, middle and upper areas of the orthosteric binding area, i.e. T94$^{3.36}$, W185$^{5.46}$, S271$^{7.42}$, H272$^{7.43}$ (lower region), L90$^{3.32}$, F168$^{5.29}$, M174$^{5.35}$, M177$^{5.38}$, L246$^{6.51}$, I249$^{6.54}$, N250$^{6.55}$, L264$^{7.35}$, I268$^{7.39}$ (middle region), V169$^{5.30}$, and I253$^{6.58}$ (upper region). These residues were mutated to alanine, and the last two also to glutamate (Table 2). For V169$^{5.30}$E and I253$^{6.58}$E receptors, the lowest-energy conformer of the glutamate side chains was retained, as indicated by the "Rapid Torsion Scan" tool available in Schrodinger suite. The double mutant V169$^{5.30}$A/W185$^{5.46}$A was also investigated. The experimental A_{2A}R - NECA (**2**) complex, the WT A_3R - NECA (**2**) complex and the 18 mutant A_3R - NECA (**2**) complexes were used for molecular docking calculations.

Optimization of docking calculations and MD simulations using the experimental structure of NECA (2) - A_{2A}R complex. To choose an efficient molecular docking method for producing the complexes between NECA (**2**), IB-MECA (**3**) and the WT or mutated A_3Rs, which would be used in the MD simulations, some established docking methods were applied to test for the correct generation of the experimental binding conformation of NECA (**2**) inside the A_{2A}R orthosteric binding area. The docking calculations of NECA (**2**) to A_{2A}R using GOLD (GOLD Suite, version 5.2; Cambridge Crystallogr. Data Cent. Cambridge, U.K., 2015; Jones et al., 1997; Verdonk et al., 2005) with ChemScore [56] and GoldScore [54] scoring functions, and Glide with Glide SP and Glide XP [57] scoring functions, showed that Glide produced a higher proportion of docking poses with NECA (**2**) having the ribose moiety faulty oriented towards the solvent-exposed part of the orthosteric binding site. In contrast, GOLD with GoldScore or ChemScore produced a higher rate of docking poses with NECA (**2**) having the ribose moiety oriented deep inside the receptor, with an RMSD of 1.5 Å compared to the X-ray coordinates of NECA (**2**) inside A_{2A}R (PDB ID 2YDV) [26]. Among the tested scoring functions, ChemScore produced the highest proportion of these docking poses. Based on this observation, the GOLD/ChemScore method was used to dock NECA (**2**) and IB-MECA (**3**) to the 19 A_3R models. The three top-scoring docking poses for each complex according to ChemScore were used for MD simulations.

MD Simulations

System Setup. To select a suitable force field for the MD simulations of the agonist-A_3R complexes, the stability of the experimental NECA (**2**) - $A_{2A}R$ complex inside 1-palmitoyl-2-oleoyl-*sn*-glycero-3-phosphoethanolamine (POPE) bilayers was tested through 150 ns MD simulations with OPLS2005 force field [51,58,59], the amber99sb force field [60,61] and the CHARMM27 force field [62]. The protein-ligand complex was inserted in a pre-equilibrated, hydrated membrane bilayer with ions using the System Builder utility of Desmond v4.9 (Desmond Molecular Dynamics System, version 3.0, D.E. Shaw Research: New York, 2011; Maestro-Desmond Interoperability Tools, version 3.1; Schrodinger: New York, 2012). More specifically, the complex was embedded in POPE bilayers consisting of ~160 lipids, including ~15,000 TIP3P water molecules [65]. Then sodium and chloride ions were placed in the water phase to neutralize the systems and reach the experimental salt concentration of 0.150 M NaCl. The orthorhombic periodic box boundaries were set 15 Å away from the protein. The total number of atoms of the complex was approximately 70,000. Desmond Viparr tool was used to assign amber99sb force field parameters [60,61] to protein and lipids, and GAFF [66] parameters to ligands. Ligand electrostatic parameters were calculated with the ANTECHAMBER module of Amber14 [67]. CHARMM27 force field parameters were also assigned with Viparr tool. To choose an appropriate force field for the MD simulations of these complexes inside POPE bilayers, we performed in duplicate a 300 ns MD simulation of NECA (**2**) - $A_{2A}R$ complex in hydrated POPE bilayers using OPLS2005 [51,58,59], CHARMM27 [62], and amber99sb [60,61] force fields. We found that amber99sb force field performed better in describing the orthosteric binding site interactions in NECA (**2**) - $A_{2A}R$ complex (PDB ID 2YDV) [26] and the α-helix conformation of TM domains 1-7 (see SI). The 300 ns MD simulations of NECA (**2**) - $A_{2A}R$ using the amber99sb force field showed that the structure of the complex adopted quickly the putative conformational features of the active form of the receptor (see SI).

MD simulations protocol. The stability of the 38 complexes, ie of NECA (**2**) or IB-MECA (**3**) and the 19 A_3R models was investigated using MD simulations for 150 ns with Desmond and amber99sb. MD simulations of the protein-ligand complexes inside the lipid bilayers were performed using the default protocol provided with Desmond v4.9. The MD simulations protocol consists of a series of MD simulations designed to relax the system, while not deviating substantially from the initial coordinates. During the first stage, a simulation was run for 200 ps at a temperature of 10 K in the NVT (constant number of particles, volume and temperature) ensemble with solute-heavy atoms restrained by a force constant of 50 kcal mol $Å^{-2}$. The temperature was raised to 310 K during a 200 ps MD simulation in the NPT (constant number of particles, pressure

and temperature) ensemble, with the same force constant applied to the solute atoms. The temperature of 310 K was used in MD simulations in order to ensure that the membrane state is above the main phase transition temperature of 298 K for POPE bilayers (Koynova and Caffrey, 1998). The heating was then followed by equilibration simulations. First, two 1 ns stages of NPT equilibration were performed. In the first 1 ns stage, the heavy atoms of the system were restrained by applying a force constant of 10 kcal mol^{-1} $Å^{-2}$, and in the second 1 ns stage, the heavy atoms of the protein-ligand complex were restrained by applying a force constant of 2 kcal mol^{-1} $Å^{-2}$ to equilibrate water and lipid molecules. In the production phase, the relaxed systems were simulated without restraints under NPT ensemble conditions for at least 150 ns. Replicas of the system were saved every 10 ps. Within this simulation time, the total energy and RMSD of the protein backbone C_α atoms reached a plateau, and the systems were considered equilibrated and suitable for statistical analysis (Tables 1, 2). Particle Mesh Ewald (PME) was employed to calculate long-range electrostatic interactions [68,69] with a grid spacing of 0.8 Å. The SHAKE method was used to constrain heavy atom-hydrogen bonds at ideal lengths and angles [70]. Van der Waals and short-range electrostatic interactions were smoothly truncated at 9.0 Å. The Nosé-Hoover thermostat [71] was utilized to maintain a constant temperature in all simulations, and the Martyna-Tobias-Klein method [72] was used to control the pressure. The equations of motion were integrated using the multistep reversible reference system propagator algorithms (RESPA) integrator [73] with an inner time step of 2 fs for bonded interactions and non-bonded interactions within a cutoff of 9 Å. An outer time step of 6.0 fs was used for non-bonded interactions beyond the cutoff. The MD simulations were performed in duplicate for the 38 complexes. All the MD simulations were run on GTX 1060 GPUs in lab workstations or on the ARIS Supercomputer. All simulations were performed using the three top-scoring docking poses for each complex as starting structures to obtain useful statistics. The visualization of produced trajectories was performed using the GUI of Maestro and the protein-ligand interaction analysis was done with the Simulation Interaction Diagram (SID) tool, available with Desmond. For hydrogen bond interactions, a distance of 2.5 Å between donor and acceptor heavy atoms, and an angle $\geq 120^o$ between donor-hydrogen-acceptor atoms and $\geq 90^o$ between hydrogen-acceptor-bonded atom were considered. Non-specific hydrophobic contacts were identified when the side chain of a hydrophobic residue fell within 3.6 Å from a ligand's aromatic or aliphatic carbon, while π-π interactions were characterized by stacking of two aromatic groups face-to-face or face-to-edge. Water-mediated interactions were characterized by a distance of 2.7 Å between donor and acceptor atoms, as well as an angle $\geq 110^o$ between donor-hydrogen-acceptor atoms and $\geq 80^o$ between hydrogen-acceptor-bonded atom.

MM-GBSA calculations. Relative binding free energies of NECA (**2**) and IB-MECA (**3**) in complex with A_3Rs were estimated using the 1-trajectory MM-GBSA approach [74] with the relevant module of Schrodinger Suite. Effective binding energies (ΔG_{eff}) were computed considering the gas phase binding energy and solvation free energy contributions to binding [75]. For this, structural ensembles were extracted in intervals of 50 ps from the last 50 ns of the production phase for each complex. Prior to the calculations, all water molecules, ions and lipids were removed, and the structures were positioned such that the geometric center of each complex was located at the coordinate origin. Molecular mechanics energies and the non-polar contribution to the solvation free energy were calculated. The polar part of the solvation free energy was determined by calculations using the Generalized-Born model. In these calculations, a dielectric constant $\varepsilon_{solute} = 1$ was assigned to the binding area and $\varepsilon_{solute} = 80$ was set for water. The effective binding free energy for each complex was calculated using the following equation:

$$\Delta G_{eff} = \Delta E_{MM} + \Delta G_{sol} \quad (1)$$

In equation (1) ΔG_{eff} is the binding free energy for each calculated complex neglecting the effect of entropic contributions or assuming them to be similar for the studied complexes. ΔE_{MM} defines the binding interaction energy between the complex, the protein and the ligand as calculated by molecular mechanics in the gas phase. ΔG_{sol} is the desolvation free energy for transferring the ligand from water in the binding area, calculated using the GBSA model. The terms ΔE_{MM} and ΔG_{sol} were calculated for each complex using equations (2) and (3)

$$\Delta E_{MM} = \Delta E_{elec} + \Delta E_{vdW} \quad (2)$$

$$\Delta G_{sol} = \Delta G_{P} + \Delta G_{NP} \quad (3)$$

In equation (2), ΔE_{elec} and ΔE_{vdW} are the electrostatic and the van der Waals interaction energies, respectively. In equation (3), ΔG_{P} is the electrostatic or polar contribution to free energy of solvation and the term ΔG_{NP} is the non-polar or hydrophobic contribution to solvation free energy. The method was implemented by the thermal_mmgbsa.py script which calculates ΔG_{eff} and its energetic contributions for a set of frames from a given trajectory using the VSGB 2.0 continuous solvation model [76]. All calculations were performed using the MD simulation trajectories that resulted from the three top-scoring docking poses for each complex to obtain useful statistics.

Biological methods

Cell culture and Transfection. Cell lines were maintained using standard protocols (European Collection of Cell Culture (ECACC)) and annually checked for mycoplasma infection using an EZ-PCR mycoplasma test kit (Biological Industries, Kibbutz Beit-Haemek, Israel). Flp-In-CHO cells (Thermo Fisher Scientific (R75807)) were grown in Hams F-12 nutrient mix supplemented with 10% FBS containing 100 μg/mL Zeocin^{TM} Selection Antibiotic (Thermo Fisher Scientific) and maintained at 37 °C with 5% CO_2, in a humidified atmosphere.

Stable Flp-In-CHO cell lines were generated in accordance with the manufacturer's instructions through co-transfection of the pcDNA5/FRT expression vector (Thermo Fisher Scientific) containing the gene of interest and the Flp recombinase expressing plasmid, pOG44 (Thermo Fisher Scientific). Transfection of cells seeded in a T25 flask at a confluency of ≥80% was performed using TransIT®-CHO Transfection Kit (MIR 2174, Mirus Bio). A total of 6 μg of DNA (receptor to pOG44 ratio of 1:9) was used at a DNA:Mirus reagent ratio of 1:3 (w/v). Stable Flp-In-CHO cell lines expressing the A_3R of interest were selected using 600 μg/mL hygromycin B (Thermo Fisher Scientific) whereby the media was changed every two days. Successful mutant cell line generation for non-signalling mutants were confirmed by Zeocin^{TM} sensitivity (100 μg/mL).

Constructs. The human A_3R (ADRA3000000, cdna.org) was sub-cloned into the pcDNA5/FRT expression vector and co-transfected with pOG44 to generation a stable Flp-In-CHO cell line. QuikChange Lightening Site-Directed Mutagenesis Kit (Agilent Technologies) was employed to generate individual mutations of the A_3R. All oligonucleotides used for mutagenesis were designed using the online Agilent Genomics 'QuikChange Primer Design' tool and purchased from Merck. All constructs were checked for faithful incorporation of the desired mutation by in-house Sanger sequencing.

Compounds. NECA (**2**) and IB-MECA (**3**), were purchased from Sigma-Aldrich and dissolved in dimethyl sulfoxide (DMSO).

cAMP accumulation assay. cAMP inhibition experiments were performed using a LANCE® cAMP kit as described previously (Weston et al., 2014; Knight et al., 2016). Briefly, Flp-In-CHO cells stably expressing WT or mutant A_3R were seeded at a density of 2,000 cells per well of a white 384-well optiplate and stimulated for 30 minutes with a range of agonist concentrations

(either of NECA (**2**) or IB-MECA (**3**)) in presence of 0.1% BSA, 25 μM rolipram and 10 μM forskolin (to enable detection of the A_3R-mediated inhibition of cAMP production) (Table S1).

Data and Statistical analysis. All *in vitro* assay data were analysed using Prism 8.0 (GraphPad software, San Diego, CA), with all dose-inhibition curves being fitted using a 3-parameter logistic equation to calculate response range and pIC_{50}. Dose-inhibition response curves (Figure S1) were normalised to either forskolin response or forskolin response relative to NECA (**2**) or IB-MECA (**3**). The data and statistical analysis comply with the recommendations on experimental design and analysis in pharmacology (Curtis et al., 2018). Statistical significance (*, *p< 0.05;**, *p<0.01;****, *p<0.001, ;*****, *p<0.0001*) was calculated using a one-way ANOVA with a Dunnett's post-test for multiple comparisons.

4 Results and Discussion

MD simulations of agonists in complex with WT A_3R. MD simulations of IB-MECA (**3**) in complex with WT A_3R for 150 ns using amber99sb revealed that the ligand is stabilized inside the orthosteric binding area through the formation of hydrogen bonds, van der Waals and π-π interactions with residues belonging to TM3, EL2, TM5, TM6 and TM7 (Figure 2). The most frequent contacts (frequency ≥ 20%) inside the receptor cavity include: (a) hydrogen bond interactions between T94$^{3.36}$ hydroxyl group and the ribose carbamide group, S271$^{7.42}$ hydroxyl group and the 2′-ribose hydroxyl group, H272$^{7.43}$ imidazole nitrogen and the 3′-ribose hydroxyl group; and two hydrogen bonds between the amide side chain of N250$^{6.55}$ and the purine 7-N and the exocyclic 6-NH group of the ligand; (b) π-π interactions between F168$^{5.29}$ and the purine aromatic ring system; (c) van der Waals interactions between L246$^{6.51}$, I268$^{7.39}$ and the purine ring system, W185$^{5.46}$, W243$^{6.48}$ and the ribose carbamide group, and between V169$^{5.30}$, L264$^{7.35}$ and the iodobenzyl group of the ligand.

The above-mentioned residues were also found to contribute similarly in the binding of NECA (**2**), with the exception of V169$^{5.30}$ and L264$^{7.35}$, since NECA has no lipophilic substituent at 6-nitrogen position to interact with these residues (Figure 2A-C, right). The MD simulations for NECA (**2**) showed an additional hydrogen bond interaction with Q167$^{5.28}$ located in the EL2 region of the receptor and a water-mediated hydrogen bond interaction with S73$^{2.65}$ which suggests a proximity of the agonist to TM2. It has been shown that when Q167$^{5.28}$ or S73$^{2.65}$ were mutated to alanine in A_3R, NECA (**2**) lost its activity (Duong et al., 2005; Almerico et al., 2013; Baltos et al., 2016).

(A)

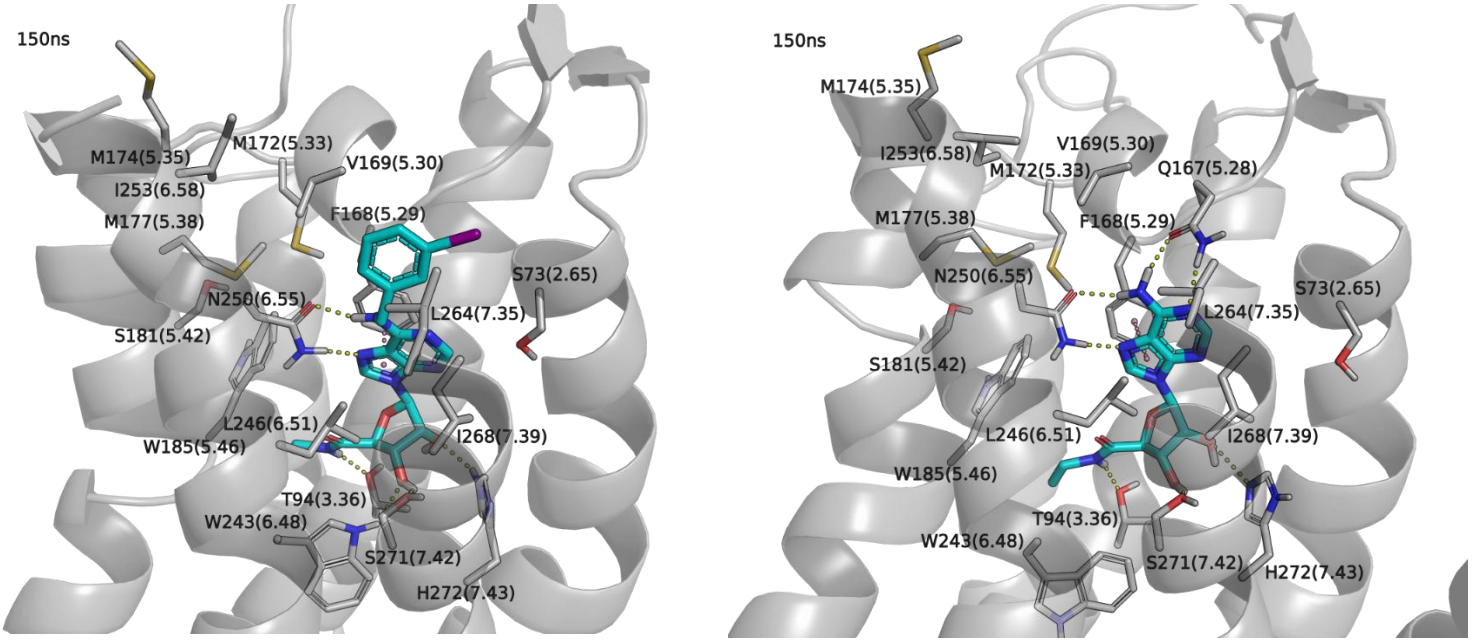
150ns
M174(5.35)
M172(5.33)
V169(5.30)
I253(6.58)
M177(5.38)
F168(5.29)
S73(2.65)
N250(6.55)
L264(7.35)
S181(5.42)
L246(6.51)
W185(5.46)
I268(7.39)
T94(3.36)
W243(6.48)
S271(7.42)
H272(7.43)
150ns
M174(5.35)
I253(6.58)
V169(5.30)
M172(5.33)
Q167(5.28)
M177(5.38)
F168(5.29)
N250(6.55)
S73(2.65)
L264(7.35)
S181(5.42)
L246(6.51)
I268(7.39)
W185(5.46)
T94(3.36)
W243(6.48)
S271(7.42)
H272(7.43)

(B)

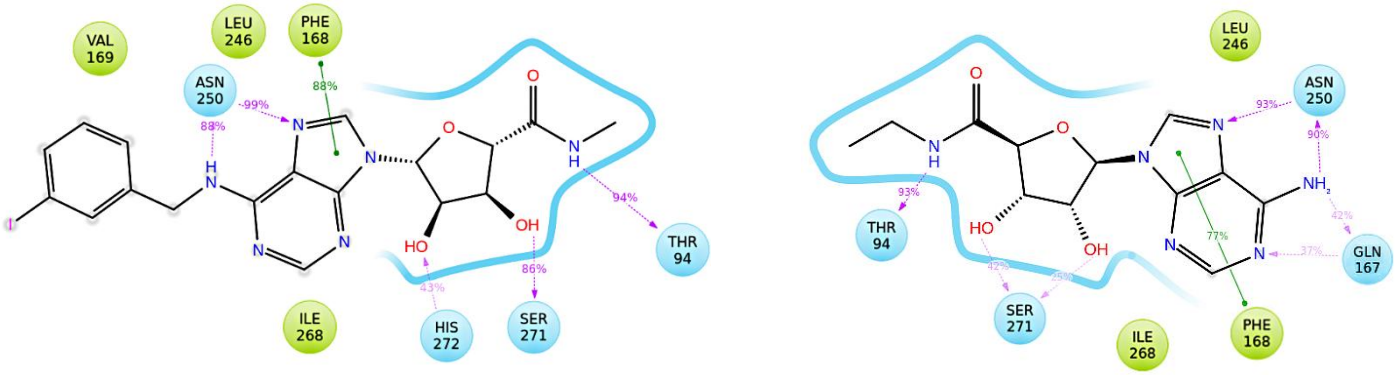
VAL 169
LEU 246
PHE 168
ASN 250
99%
88%
88%
94%
THR 94
ILE 268
HIS 272
SER 271
43%
86%
HO
OH
LEU 246
ASN 250
93%
90%
93%
THR 94
HO
OH
42%
25%
SER 271
ILE 268
PHE 168
77%
37%
42%
GLN 167

(C)

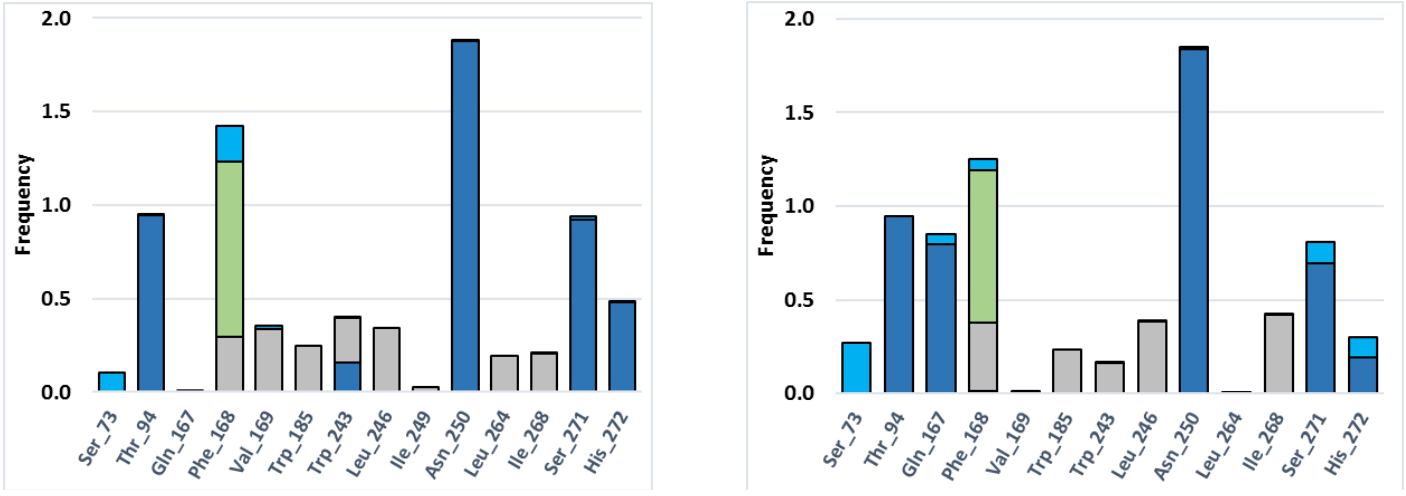
Frequency
2.0
1.5
1.0
0.5
0.0
Ser_73
Thr_94
Gln_167
Phe_168
Val_169
Trp_185
Trp_243
Leu_246
Ile_249
Asn_250
Leu_264
Ile_268
Ser_271
His_272
Frequency
2.0
1.5
1.0
0.5
0.0
Ser_73
Thr_94
Gln_167
Phe_168
Val_169
Trp_185
Trp_243
Leu_246
Asn_250
Leu_264
Ile_268
Ser_271
His_272

Figure 2. (A) Snapshot of IB-MECA (**3**) (left) and NECA (**2**) (right) inside the orthosteric binding area of WT A_3R at 150 ns of MD simulation, (B) 2D interaction diagram and (C) receptor-ligand interaction histogram for IB-MECA (**3**) (left) and NECA (**2**) (right) inside the orthosteric binding area of WT A_3R for 0-150 ns of MD simulations. Bars are plotted for residues with interaction frequencies ≥ 0.2 for either IB-MECA (**3**) or NECA (**2**). Color scheme (A): Ligand=cyan sticks, receptor=grey ribbon and sticks, H-bond interactions=yellow dashes, π-π interactions=pink dashes; Color scheme (B): polar surface/residues=blue, hydrophobic residues=green; Color scheme (C): H-bond interactions=dark blue, hydrophobic interactions=grey, π-π interactions=green, water-mediated interactions=light blue.

Biological results and biomolecular simulations interpretation

Mutagenesis and functional assays results. We investigated the significance of residues with the most frequent interactions with IB-MECA (**3**) and NECA (**2**) in the orthosteric binding area of WT A_3R, by assessing both experimentally and computationally the effect of a mutation to the stability of the agonist-A_3R complex. Residues L90$^{3.32}$, M174$^{5.35}$, M177$^{5.38}$, and I253$^{6.58}$ were also examined due to their proximity to the bound agonists (Figure 3). Experimentally, we applied a functional assay which quantified the level of activation of WT and mutant A_3Rs by measurement of the intracellular cAMP levels (Table 2, Table S1, Figure S1). This marker reflects the effectiveness of signal transduction initiated by the interaction of IB-MECA (**3**) or NECA (**2**) with the orthosteric binding area. Besides the hitherto unexplored binding site residues, the studied mutations to alanine also included the previously explored residues T94$^{3.36}$, M177$^{5.38}$, N250$^{6.55}$, S271$^{7.42}$ and H272$^{7.43}$ [37,39] with the intention to test for consistency between ligand binding and signal transduction. Residues T94$^{3.36}$, M177$^{5.38}$, W243$^{6.48}$, N250$^{6.55}$, S271$^{7.42}$ and H272$^{7.43}$ were previously found to be critically involved in agonist binding [37,39,81]. Mutation of residue H272$^{7.43}$ to glutamic acid has been previously shown to result in a 19-fold decreased activity of NECA (**2**) compared to the WT receptor [82,83]. We have recently shown that our applied assay is in agreement with binding affinity results. (Barkan, K.; Lagarias, P.; Vrontaki, E.; Stamatis, D.; Hoare, S.; Klotz, K.-N.; Kolocouris, A.; Ladds, G. Pharmacological Characterisation of Novel Adenosine Receptor A3R Antagonists. Preprint.)

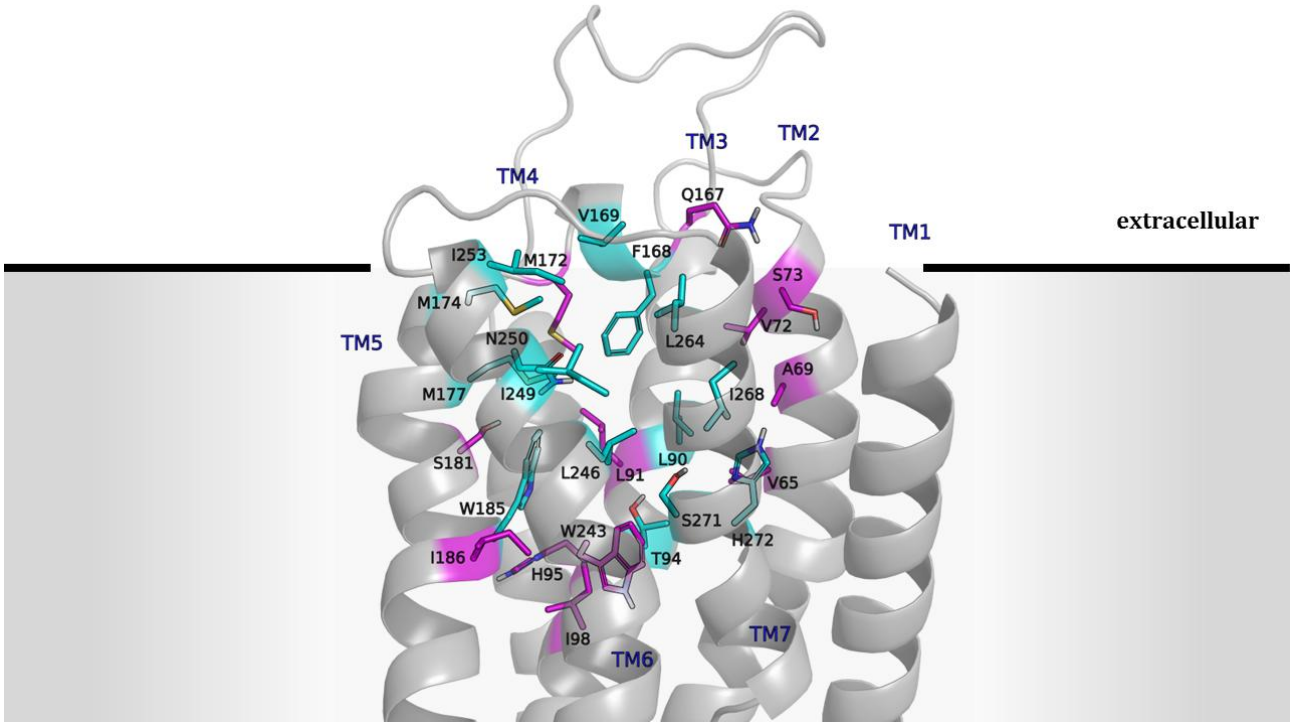

Figure 3. Orhosteric binding area of WT A_3R according to IB-MECA (**3**) – receptor complex (residues within 5 Å of the ligand). Residues mutated in this study are illustrated in cyan sticks, while the rest are illustrated in magenta sticks. Lipid bilayer is represented by the grey background.

The experiments revealed mutations that increase the activity of at least one agonist ($V169^{5.30}A$, $V169^{5.30}E$, $M174^{5.35}A$, $I249^{6.54}A$, $V169^{5.30}A/W185^{5.46}A$), reduce the activity of at least one agonist ($L90^{3.32}A$, $M174^{5.35}A$, $M177^{5.38}A$), negate agonist activity ($T94^{3.36}A$, $F168^{5.29}A$, $L246^{6.51}A$ $N250^{6.55}A$, $I268^{7.39}A$, $S271^{7.42}A$, $H272^{7.43}A$), have a mixed effect on agonist activity ($M174^{5.35}A$), or have a very small or no effect on agonist activity ($W185^{5.46}A$, $I253^{6.58}A$, $I253^{6.58}$Eand $L264^{7.35}A$). MD simulations of the latter mutant receptors uncovered novel interactions with proximate residues to the binding area, including hydrogen bond interactions with $S73^{2.65}$, $S181^{5.42}$ and van der Waals interactions with $M172^{5.33}$, $M174^{5.35}$, $M177^{5.38}$ and $I253^{6.58}$.

We identified residues with an agonist-specific effect on signaling. In particular, mutations $V169^{5.30}A$ and $I249^{6.54}A$ resulted correspondingly to increased and unchanged agonist potency for IB-MECA (**3**) compared to the WT A_3R receptor. These mutations produced an opposite effect for NECA (**2**), i.e. an unchanged and an increased agonist potency when compared to the WT A_3R receptor.

MM-GBSA binding free energy calculations. To investigate computationally the stability and the interactions for each mutant A_3R-agonist complex, 150 ns MD simulations were performed for the

complexes between IB-MECA (**3**) or NECA (**2**) and the 18 mutant A_3Rs. Binding free energy calculations of agonists in complex with A_3Rs were performed using the MM-GBSA method. The experimentally determined pIC_{50} values and the calculated ΔG_{eff} values showed significant correlation for both IB-MECA (**3**) and NECA (**2**) (Table S3, Figure S2), with r = -0.69 (95% confidence interval, -0.91 to -0.19, $p < 0.05$) and r = -0.76 (95% confidence interval, -0.93 to -0.33, $p < 0.01$), respectively (Figure 4).

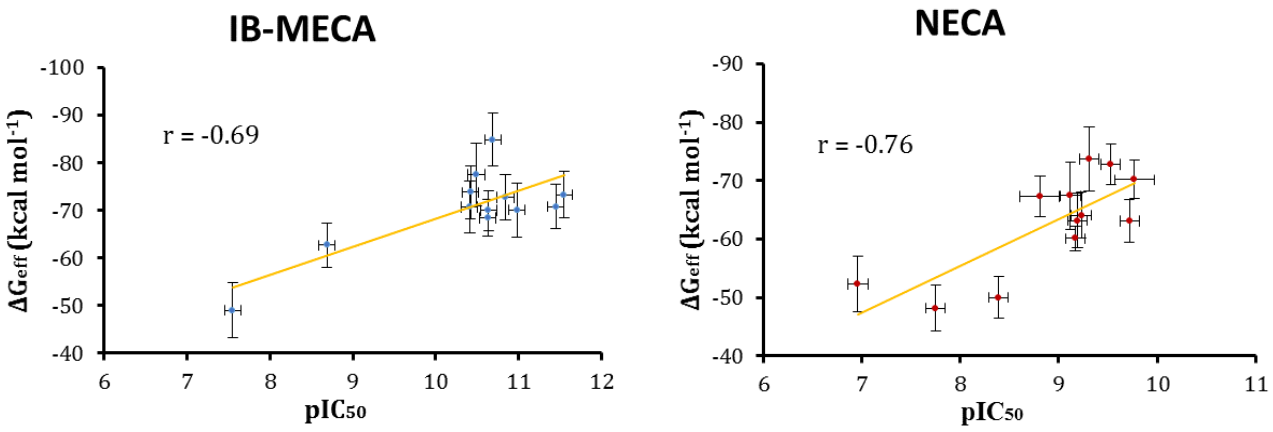

Figure 4. Binding free energies of IB-MECA (**3**) and NECA (**2**) computed by the MM-GBSA method (ΔG_{eff}) plotted against experimental activities (pIC_{50}) for several mutant A_3Rs.

We observed that mutants which led to reduction or loss of agonist activity display relative binding free energy values ($\Delta\Delta G_{eff} = \Delta G_{eff,mut} - \Delta G_{eff,WT}$) for the studied agonist greater than +20 kcal mol^{-1} compared to the WT receptor; in fact, most of them are larger than + 30 kcal mol^{-1} (Table 2, Figure S3). Mutants L90$^{3.32}$A, T94$^{3.36}$A, F168$^{5.29}$A, M177$^{5.38}$A, L246$^{6.51}$A, N250$^{6.55}$A, I268$^{7.39}$A, S271$^{7.42}$A and H272$^{7.43}$A led to reduction or loss of activity for both IB-MECA (**3**) and NECA (**2**), and M174$^{5.35}$A only for NECA (**2**). On the other hand mutant receptors that maintain or increase activity of the studied agonist have binding free energy values that were 1-15 kcal mol^{-1} more positive than this agonist-WT A_3R; most of them differ by less than +10 kcal mol^{-1} (Table 2, Figures S2-S3). Mutants V169$^{5.30}$E, W185$^{5.46}$A, I249$^{6.54}$A, I253$^{6.58}$A, I253$^{6.58}$E, L264$^{7.35}$A and V169$^{5.30}$A/W185$^{5.46}$A that maintain or increase activity for at least one agonist (Table 2). A more accurate computational method, like the FEP [42] should produce $\Delta\Delta G_{eff}$ values around zero or negative values for mutant receptors showing increase signaling. Additionally, it was not possible to distinguish between receptors that maintain, and receptors that increase, agonist activity based on the $\Delta\Delta G_{eff}$ values taken from MM-GBSA. Nevertheless, the MM-GBSA values for inactive or less active receptor are clearly more positive than receptors that maintain WT activity or increased activity and can be useful for the interpretation of the mutagenesis results.

Table 2. Agonistic activities, ligand displacement (RMSD in Å) from its starting position in MD simulations of IB-MECA (3) or NECA (2) in complex with WT and mutant A_3Rs, and MM-GBSA calculated relative binding free energies ($\Delta\Delta G_{eff}$ in kcal mol^{-1}).

N/N	Mutants (Region)	IB-MECA (3)					NECA (2)				
		$\Delta\Delta G_{eff}$ [1]	pIC_{50}	Receptor RMSD [2]	Ligand RMSD [3]	Potency	$\Delta\Delta G_{eff}$ [1]	pIC_{50}	Receptor RMSD [2]	Ligand RMSD [3]	Potency
1	**WT** (-)	0	10.64 ±0.1	2.58±0.13	1.47±0.41	baseline	0	8.94 ±0.1	2.43±0.36	1.65±0.26	baseline
2	**L90$^{3.32}$A** (Low)	22.18	8.67 ±0.1	2.79±0.19	3.48±0.37	decrease	26.17	7.81 ±0.1	4.43±0.59	5.46±0.85	decrease
3	**T94$^{3.36}$A** (Low)	42.33	NR [4]	3.23±0.14	4.58±0.55	-	39.4	NR [4]	4.50±0.38	4.31±1.20	-
4	**F168$^{5.29}$A** (Middle)	37.02	NR [4]	2.91±0.13	5.94±1.31	-	39.8	NR [4]	3.93±0.52	4.54±0.67	-
5	**V169$^{5.30}$A** (Upper)	14.77	11.23 ±0.1	2.37±0.15	3.17±0.28	increase	0.67	9.31 ±0.1	2.11±0.21	1.93±0.14	normal
6	**V169$^{5.30}$E** (Upper)	10.27	11.48 ±0.1	2.28±0.10	1.83±0.17	increase	11.27	9.68 ±0.1	2.55±0.46	1.96±0.22	increase
7	**M174$^{5.35}$A** (Middle)	14.86	11.01 ±0.1	2.70±0.17	2.12±0.27	increase	24.32	8.42 ±0.1	2.8±0.36	5.65±0.23	decrease
8	**M177$^{5.38}$A** (Middle)	35.85	7.64 ±0.1	2.80±0.17	5.29±0.90	decrease	22.01	6.96 ±0.1	2.5±0.25	2.65±0.45	decrease
9	**W185$^{5.46}$A** (Low)	16.43	10.64 ±0.1	2.66±0.22	2.30±0.19	normal	13.25	9.21 ±0.1	2.36±0.36	3.08±0.58	normal
10	**L246$^{6.51}$A** (Middle)	30.87	NR [4]	2.82±0.20	5.01±0.46	-	24.38	NR [4]	4.02±0.57	2.94±0.67	-
11	**I249$^{6.54}$A** (Middle)	7.31	10.67 ±0.1	2.78±0.16	3.14±0.22	normal	1.52	9.53 ±0.1	2.68±0.18	3.92±0.20	increase

12	**N250$^{6.55}$A** (Middle)	20.23	NR [4]	2.89±0.15	5.75±0.22	-	30.95	NR [4]	2.22±0.31	2.03±0.19	-
13	**I253$^{6.58}$A** (Upper)	14.16	10.31 ±0.1	2.89±0.10	3.85±0.35	normal [5]	7.01	8.92 ±0.2	2.44±0.32	1.52±0.39	normal
14	**I253$^{6.58}$E** (Upper)	12.12	10.84 ±0.1	2.30±0.16	4.23±0.25	normal [5]	10.27	9.23 ±0.1	2.44±0.35	3.26±0.29	normal
15	**L264$^{7.35}$A** (Middle)	9.6	10.29 ±0.1	2.72±0.17	2.00±0.33	normal [5]	8.60	9.11 ±0.1	2.68±0.27	3.02±0.35	normal
16	**I268$^{7.39}$A** (Middle)	29.43	NR [4]	3.28±0.17	9.42±0.34	-	27.33	NR [4]	4.16±0.42	2.52±1.01	-
17	**S271$^{7.42}$A** (Low)	38.69	NR [4]	2.82±0.13	5.13±0.68	-	29.67	NR [4]	3.58±0.31	3.26±0.76	-
18	**H272$^{7.43}$A** (Low)	21.85	NR [4]	3.46±0.21	2.71±0.36	-	26.88	NR [4]	3.28±0.29	6.27±0.87	-
19	**V169$^{5.30}$A/ W185$^{5.46}$A** (Upper/Low)	14.05	11.45 ±0.1	2.66±0.11	2.78±0.24	increase	4.15	9.59±0.1	2.42±0.24	2.20±0.57	increase

[1] Relative binding free energy (kcal mol $^{-1}$) between mutant and WT receptors ($\Delta G_{\text{eff, mutant}} - \Delta G_{\text{eff, WT}}$). ΔG_{eff} is calculated from the last 50 ns of the trajectories using 50 ps intervals (i.e. 1000 frames per trajectory). See also Table S3.

[2] Mean±SD (Å). Protein RMSD is calculated for the C_α atoms of the α-helices, for the last 50 ns of the trajectories. Frame 0 is used as reference structure.

[3] Mean±SD (Å). Ligand RMSD is calculated after superposition of each protein-ligand complex to that of frame 0 (reference structure) based on the C_α atoms of the protein, for the last 50ns of the trajectories.

[4] NR, no response.

[5] A cutoff of more than 0.5 should be considered as a change.

Mutations that led to loss or reduction in signal transduction for both IB-MECA (3) and NECA (2). Our biological assay results were in agreement with previously reported binding affinity results (Gao et al., 2003, 2002a, 2002b), showing no detectable signaling for T94$^{3.36}$A, N250$^{6.55}$A, S271$^{7.42}$A and H272$^{7.43}$A A_3R mutants, most likely due to loss of IB-MECA (**3**) and NECA binding (**2**). In addition to these residues, our experiments revealed that F168$^{5.29}$A, L246$^{6.51}$A and I268$^{7.39}$A mutants led to no detectable response upon stimulation with IB-MECA (**3**) or NECA (**2**) (Table 2). Furthermore, we observed that when the indirectly-interacting residues L90$^{3.32}$ and M177$^{5.38}$ were mutated to alanine the signaling was decreased for both agonists.

Visual inspection of the MD simulation trajectories for T94$^{3.36}$A, F168$^{5.29}$A, L246$^{6.51}$A, N250$^{6.55}$A, I268$^{7.39}$A and S271$^{7.42}$A A_3Rs showed that IB-MECA (**3**) makes sparse contacts with various residues inside the binding area, resulting in weak, transient interactions (Figure S4) and unstable binding positions compared to those observed for the WT A_3R-agonist complexes. This is described by the high ligand RSMD values which ranged from ca 5-10 Å for the mutant A_3R-IB-MECA (**3**) complexes, compared to only 1.5 Å for WT A_3R-IB-MECA (**3**) (Figure S5). The significant drift of the agonist from its starting binding position is reflected also by a ca 21-42 kcal mol^{-1} binding free energy loss compared to the WT receptor (Table 2, Figures S2-S3). For example, the MD simulations of L246$^{6.51}$A A_3R suggest that the mutation causes IB-MECA (**3**) to lose stabilizing interactions and rotate around the z-axis by ca 180º relative to its starting position (Figure 5) resulting in an RMSD of ca 5 Å and a $\Delta\Delta G_{eff}$ of ca +31 kcal mol^{-1}. The results for L246$^{6.51}$A A_3R show that while NECA (**2**) does not drift significantly from its starting position (ligand RMSD ca 2.9 Å) it is destabilized by abolishing the hydrogen bond and π-π interactions between the purine heterocycle and N250$^{6.55}$ or F168$^{5.29}$, respectively (Figure 5). In the case of NECA (**2**) against L246$^{6.51}$A, N250$^{6.55}$A, I268$^{7.39}$A,and S271$^{7.42}$A A_3Rs, and of IB-MECA (3) against H272$^{7.43}$A A_3R, although the ligand RMSD values are 2-3.3 Å, the binding free energy is still ca +24-30 kcal mol^{-1} more positive compared to the WT receptor. According to the analysis of our MD simulations, this results from the loss of important agonist-receptor interactions (Figure S4).

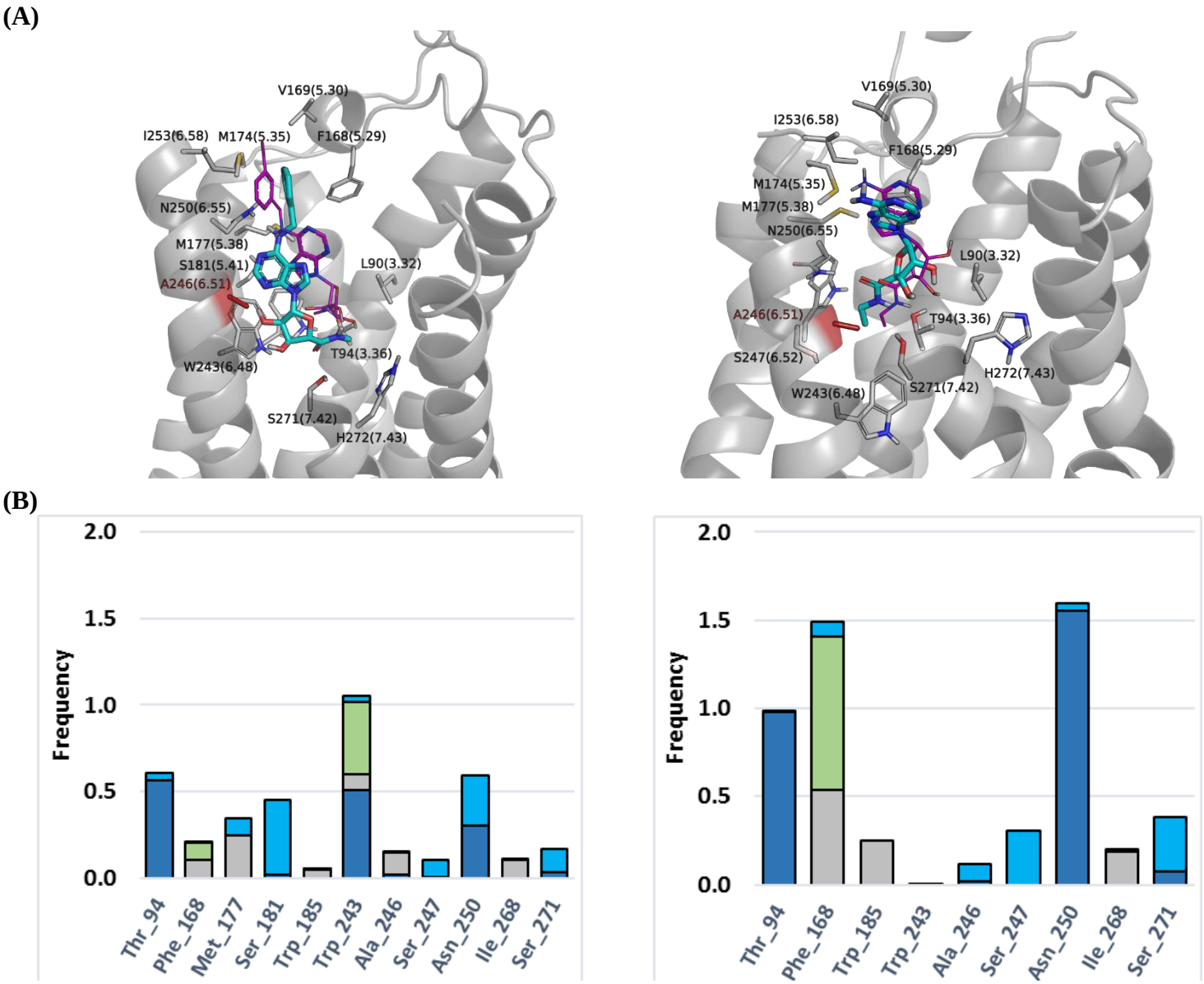

Figure 5. (A) Snapshots of IB-MECA (**3**) (left) and NECA (**2**) (right) inside the L246$^{6.51}$A A_3R binding site at 0 ns (ligand carbons in magenta) and 150 ns of MD simulation (ligand carbons in cyan); Color scheme: (A) receptor=grey ribbon and sticks; (B) polar surface/residues=blue, hydrophobic residues=green; Color scheme (C): H-bond interactions=dark blue, hydrophobic interactions=grey, π-π interactions=green, water-mediated interactions=light blue. Mutation in TM6 is shown in red sticks and ribbon.

The ligand RMSD values is ca 3.5 Å for IB-MECA (**3**) in complex with the L90$^{3.32}$A receptor, and although higher than the ligand RMSD for the WT A_3R complex, the agonist is accommodated inside the orthosteric binding site (Table 2, Figures S4-S6). The interaction plots from the MD simulations, along with the +22 kcal mol^{-1} higher ΔG_{eff}, reflect the reduced activity of IB-MECA (**3**) for L90$^{3.32}$A A_3R. The simulations suggest that the important hydrogen bond interactions with S271$^{7.42}$ and H272$^{7.43}$ seen for the WT receptor are reduced and replaced by water-mediated interactions, while the most important reduction is recorded for the significant π-π interaction with

F168$^{5.29}$; new interactions appeared including for example M177$^{5.38}$ (Figures 6, S6). NECA (**2**) drifted considerably from its starting binding conformation, having an average ligand RMSD value of ca 5.5 Å which is in agreement with the $\Delta\Delta G_{eff}$ value of ca +26.2 kcal mol^{-1} compared to the WT A_3R (Figures S5, S6). In contrast, NECA (**2**) did not drift significantly from its initial binding position inside the orthosteric binding area of M177$^{5.38}$A A_3R, with an average ligand RMSD value of ca 2.7 Å. Nevertheless, the +22 kcal mol^{-1} higher ΔG_{eff} compared to the WT A_3R is indicative of a reduced activity; IB-MECA (**3**) inside M177$^{5.38}$A A_3R showed high RMSD and +22 kcal mol^{-1} higher ΔG_{eff} (SI, Figure S7). It seems that residues L90$^{3.32}$ or M177$^{5.38}$, which are correspondingly located deep in the binding area or close to the end of EL2, in a distance of ca 4 Å or 5 Å away from the ligand (Figure 2), facilitate agonist affinity through indirect interactions by modulating binding area conformation. The interactions of NECA (**2**) with M177$^{5.38}$A, L246$^{6.51}$A, N250$^{6.55}$A, I268$^{7.39}$A, S271$^{7.42}$A, and of IB-MECA (**3**) with L90$^{3.32}$A and H272$^{7.43}$A A_3Rs are exemplary cases where simple inspection of the trajectories, the RMSD values, or even of the interaction plots cannot account for the binding conformation stability of the agonists, but more detailed analysis is needed, for example through binding free energy calculations.

(A)

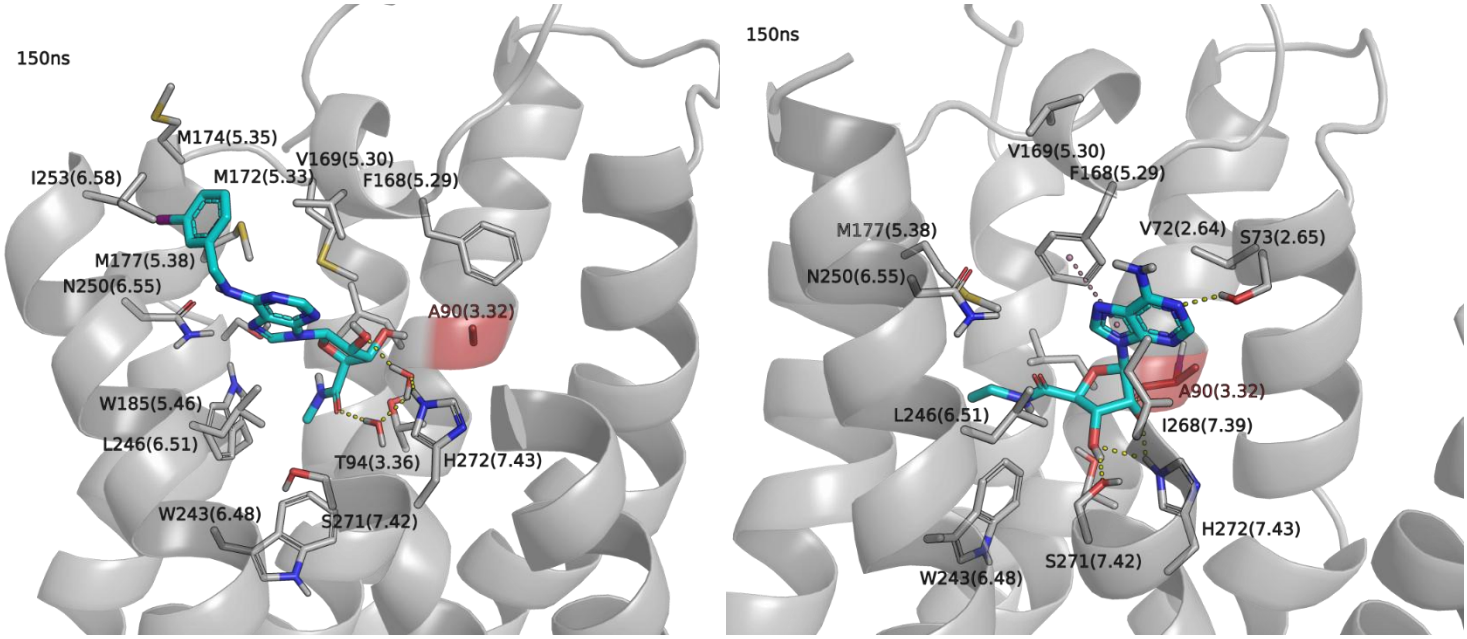

(B)

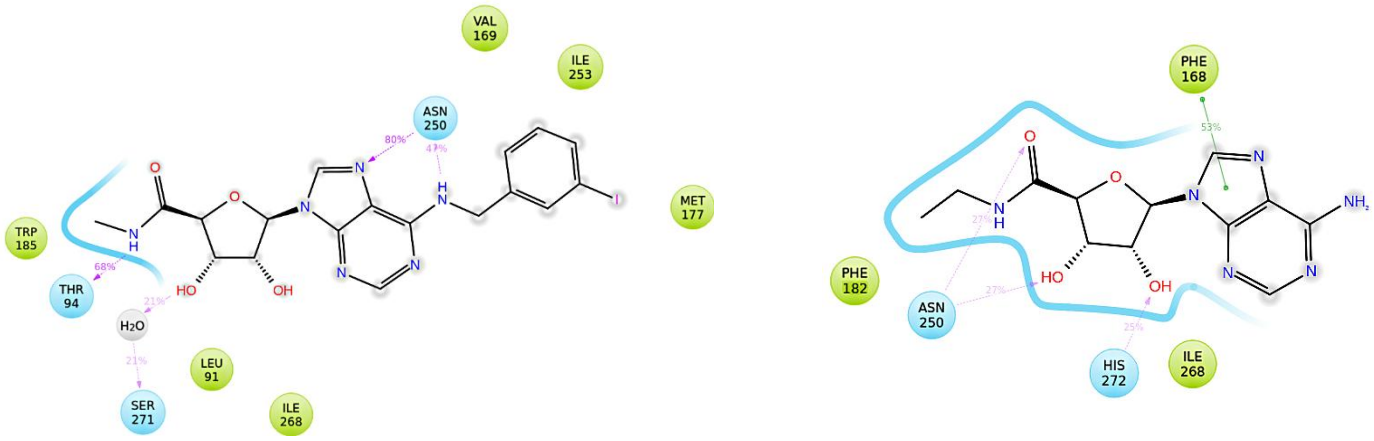

(C)

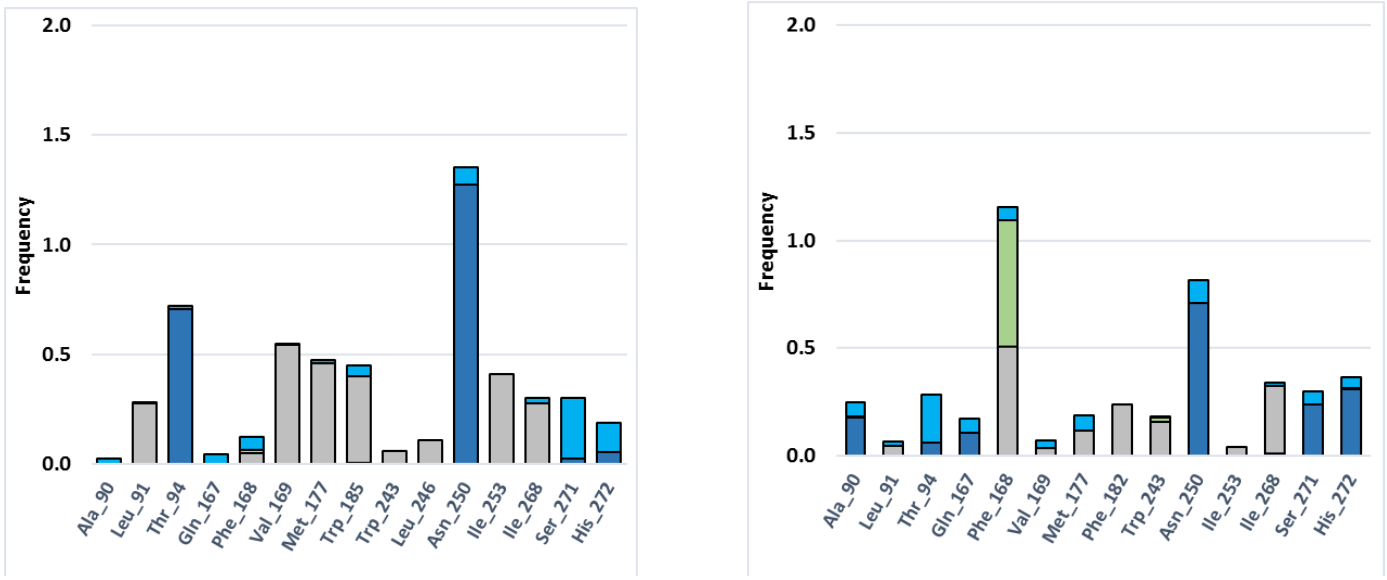

Figure 6. (A) Snapshot of IB-MECA (**3**) (left) and NECA (**2**) (right) inside the L90$^{3.32}$A A_3R binding site at 150 ns of MD simulation, (B) 2D interaction diagram, and (C) receptor-ligand interaction histogram for IB-MECA (left) and NECA (right) inside L90$^{3.32}$A A_3R orthosteric binding area, recorded from 0-150 ns of MD simulation trajectories. Color scheme (A): Ligand=cyan sticks, receptor=white ribbon and sticks, H-bond interactions=yellow dashes, π-π interactions=pink dashes; Color scheme (B): polar surface/residues=blue, hydrophobic residues=green; Color scheme (C): H-bond interactions=dark blue, hydrophobic interactions=grey, π-π interactions=green, water-mediated interactions=light blue. Mutation in TM3 is shown in red sticks and ribbon.

Mutation M174$^{5.35}$A has opposite effect on signal transduction for each agonist. The mutant M174$^{5.35}$A, in contrast to NECA (**2**), displaced an increase in the activity of IB-MECA (**3**), which is consistent with the simulated stability of the agonist inside the binding area of the WT receptor having an RMSD value of 2.15 Å. This is most likely due to the frequent interactions of the iodobenzyl substituent with other lipophilic residues of this area, such as V169$^{5.30}$ and M177$^{5.38}$. Other frequently interacting residues are T94$^{3.36}$, F168$^{5.29}$, W185$^{5.46}$, W243$^{6.48}$, L246$^{6.51}$, N250$^{6.55}$

and I268$^{7.39}$ (Figure S8). The reduced activation upon stimulation with NECA (**2**) is possibly caused by changes in the conformational area, since M174$^{5.35}$ is not directly involved in interactions with the agonist but is next to residues in contact with the agonists. The MD simulations suggest that for NECA (**2**)-M174$^{5.35}$A A_3R, most of the standard interactions are lost or reduced, and sparse new interactions - mainly water-mediated - appeared (Figure S8), which are reflected by the high ligand RMSD value of 5.65 Å and $\Delta\Delta G_{eff}$ of ca +24 kcal mol^{-1}.

Mutations that maintain signal transduction for both agonists. The mutations W185$^{5.46}$A, I253$^{6.58}$A and L264$^{7.35}$A did not change significntly receptor activity levels for IB-MECA **(3)** and NECA **(2)** compared to the WT A_3R, suggesting that residues W185$^{5.46}$, I253$^{6.58}$ and L264$^{7.35}$ are not critical for receptor stimulation from these agonists. The MD simulations of IB-MECA (**3**) or NECA (**2**) - W185$^{5.46}$A A_3R complex show similarities to the binding profile of the agonist to the WT receptor. New frequent interactions are recorded with residues not participating in direct interactions with the WT receptor, i.e. with M177$^{5.38}$ in both agonist complexes and with S181$^{5.42}$ in the NECA (**2**) complex (Figure S9). The simulations suggest that the hydrogen bonds between S271$^{7.42}$, H272$^{7.43}$ and NECA (**2**), present in the WT A_3R, become stable water-mediated hydrogen bond interactions in W185$^{5.46}$A, I253$^{6.58}$A and L264$^{7.35}$A A_3R-NECA (**2**) complexes (SI, Figures S9-S11).

Mutations that increase signal transduction for one of the agonists. Our MD simulations suggest that IB-MECA (**3**) inside V169$^{5.30}$A A_3R maintains interactions with T94$^{3.36}$, F168$^{5.29}$, N250$^{6.55}$, L246$^{6.51}$, S271$^{7.42}$ and H272$^{7.43}$. This mutation increases considerably the space close to the changed residue A169$^{5.30}$ and enables IB-MECA (**3**) to relocate towards TM5 and TM6, making new favorable lipophilic interactions with residues of that area. The agonist engages in closer hydrophobic contacts with residues of EL2, TM5 and TM6, such as A169$^{5.30}$, M177$^{5.38}$, W185$^{5.46}$ and I253$^{6.38}$ via its iodobenzyl and methylcarbamide substituents which result in the increased activity of the agonist (Table 2). The increased volume of the binding area allowed the appearance of more water-mediated interactions, e.g. with H272$^{7.43}$ and S73$^{2.65}$. On the other hand, NECA (**2**) maintains standard interactions observed also in the WT A_3R complex and forms an additional hydrogen bond interaction with L90$^{3.32}$, which presumably result in WT-like activity (Table 2).

Compared to the activity against WT A_3R, NECA (**2**) has also increased potency against I249$^{6.54}$A A_3R, while the potency of IB-MECA (**3**) is preserved. In contrast to the case of NECA (**2**), the M174$^{5.35}$A mutant effected an increase in the activity of IB-MECA (**3**) (see SI, Figures S12 and S8 respectively).

(A)

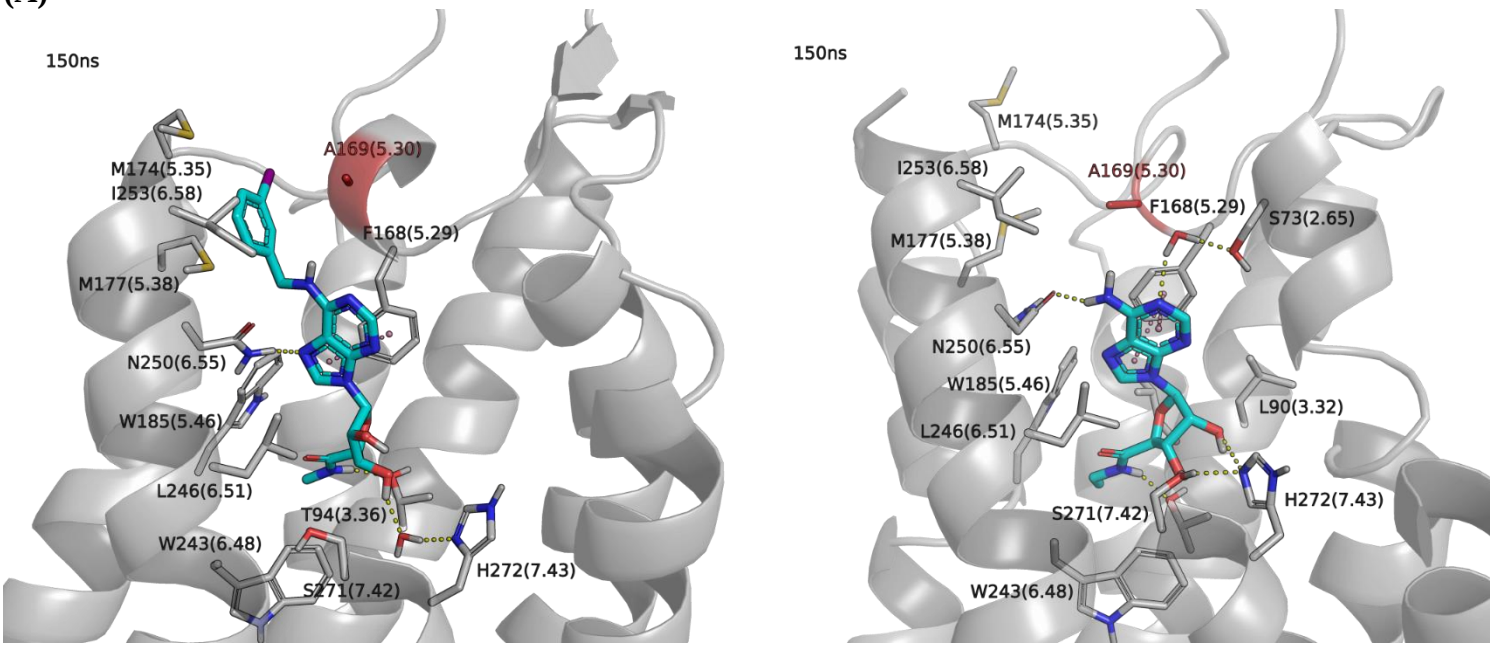
150ns
M174(5.35)
I253(6.58)
A169(5.30)
F168(5.29)
M177(5.38)
N250(6.55)
W185(5.46)
L246(6.51)
T94(3.36)
W243(6.48)
S271(7.42)
H272(7.43)
150ns
M174(5.35)
I253(6.58)
A169(5.30)
F168(5.29)
S73(2.65)
M177(5.38)
N250(6.55)
W185(5.46)
L90(3.32)
L246(6.51)
H272(7.43)
S271(7.42)
W243(6.48)

(B)

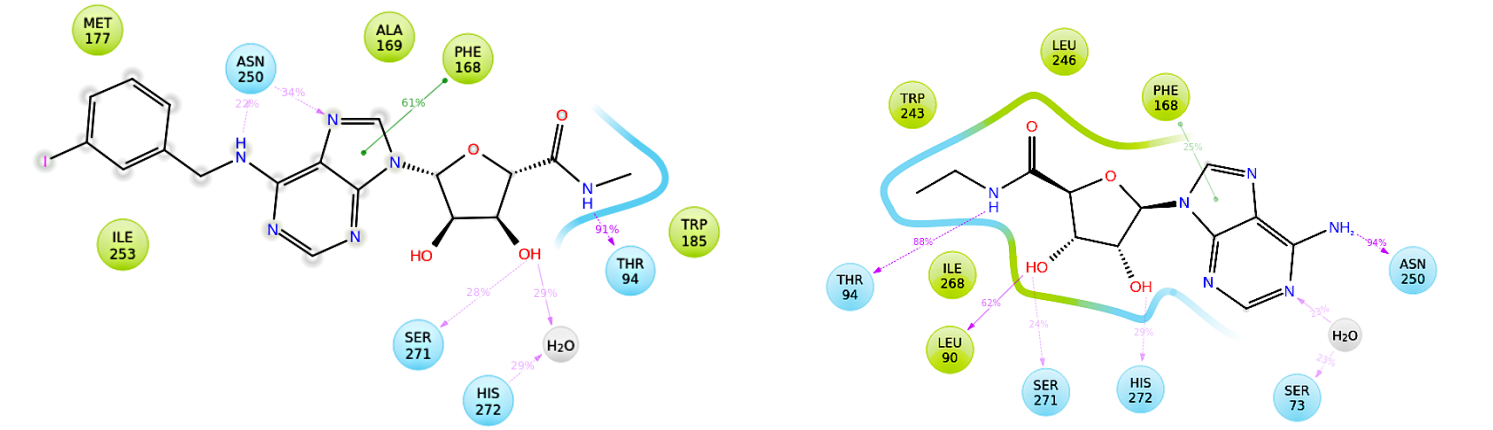
MET 177
ASN 250
ALA 169
PHE 168
ILE 253
TRP 185
THR 94
SER 271
HIS 272
H2O
LEU 246
TRP 243
PHE 168
THR 94
ILE 268
LEU 90
SER 271
HIS 272
SER 73
ASN 250
H2O

(C)

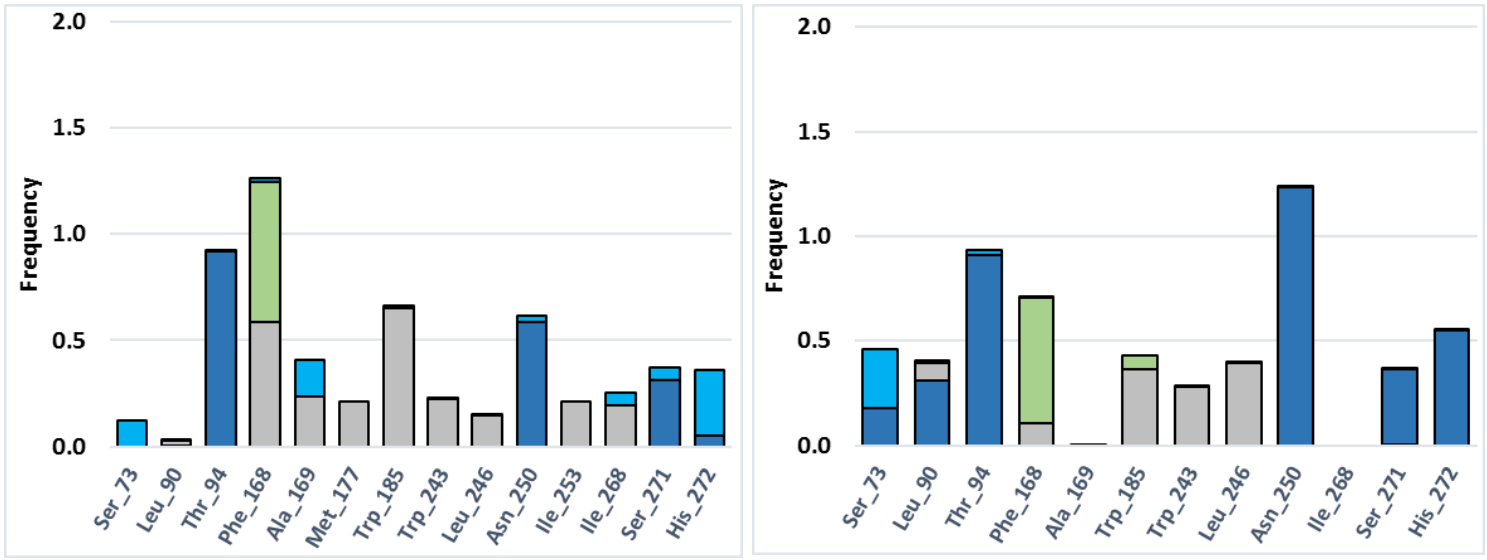
Frequency
2.0
1.5
1.0
0.5
0.0
Ser_73
Leu_90
Thr_94
Phe_168
Ala_169
Met_177
Trp_185
Trp_243
Leu_246
Asn_250
Ile_253
Ile_268
Ser_271
His_272
Frequency
2.0
1.5
1.0
0.5
0.0
Ser_73
Leu_90
Thr_94
Phe_168
Ala_169
Trp_185
Trp_243
Leu_246
Asn_250
Ile_268
Ser_271
His_272

Figure 7. (A) Snapshot of IB-MECA (**3**) (left) and NECA (right) (**2**) inside the binding site of V169$^{5.30}$A A_3R at 150 ns of MD simulation, (B) 2D interaction diagram and receptor-ligand interaction histogram for IB-MECA (left) and NECA (right) inside V169$^{5.30}$A A_3R orthosteric binding area, recorded from 0-150 ns of MD simulation trajectories. Color scheme (A): Ligand=cyan sticks, receptor=white ribbon and sticks, H-bond interactions=yellow dashes, π-π interactions=pink dashes; Color scheme (B): polar surface/residues=blue, hydrophobic residues=green; Color scheme (C): H-bond interactions=dark blue, hydrophobic interactions=grey, π-π interactions=green, water-mediated interactions=light blue. Mutation in shown with a red color in the ribbon of EL2.

Mutations that increase signal transduction for both agonists. Our simulations show an increased interaction fraction with W185$^{5.46}$ in the IB-MECA (**3**) - V169$^{5.30}$A A_3R complex (Figure 7) and with V169$^{5.30}$ in the IB-MECA (**3**) - W185$^{5.46}$A A_3R complex (Figure S11). Thus, we considered and tested the hypothesis that these two residues act synergistically in the binding of IB-MECA (**3**) by changing both residues to alanine. These two mutations increase the available space at the upper and lower region of the binding area. The functional assays for this double mutant indicated an overactive receptor, when stimulated with NECA (**2**) or IB-MECA (**3**) most likely due to the V169$^{5.30}$A mutation (Table 2). In the course of the MD simulations, IB-MECA (**3**)-V169$^{5.30}$A/W185$^{5.46}$A A_3R complex preserves the important hydrogen bond interactions with T94$^{3.36}$, N250$^{6.55}$ and S271$^{7.42}$ but not with H272$^{7.43}$. A new strong hydrogen bond interaction is formed between S181$^{5.42}$ on TM5 and the carboxamide group of the agonist, spanning the entirety of the trajectories (Figure S13). This hydrogen bond causes the agonist to move substantially towards TM6 with an RMSD value of 2.66 Å and lose the π-π interaction with F168$^{5.29}$, which is partly compensated by new frequent contacts with L91$^{3.33}$ and M172$^{5.33}$ through the iodobenzylpurine moiety of IB-MECA (**3**). NECA (**2**) is engaged in a similar set of intermolecular interactions but maintaining π-π interactions with F168$^{5.29}$ its RMSD value is 2.20 Å and forms a new hydrophobic interaction with I98$^{3.40}$. Although this kind of structural changes need experimental verification, the MD simulations suggest a plasticity of the ligand area which enables the binding area to change compared to V169$^{5.30}$A A_3R due to the additional W185$^{5.46}$A mutation.

Mutations to glutamic acid. A_3R has a unique lipophilic area in-between EL2, TM5 and TM6 which has the characteristic residue V169$^{5.30}$, while A_1R and A_{2A}R and A_{2B}R have a glutamic acid residue in the same position. It is speculated that residue (5.30) may be linked to the subtype-selectivity of IB-MECA (**3**) and its correct modeling can be used in drug design for the identification of new A_3R-selective agonists and antagonists. This is presumably due to the lipophilic iodobenzyl moiety of IB-MECA (**3**) which likely fits in a lipophilic area formed around V169$^{5.30}$. It has been generally suggested that differences in the residues of the upper region give

rise to the selectivity of ligands against a particular AR subtype [85]. Residue I253$^{6.58}$ also lies in this area but does not interact directly with the agonists according to the MD simulation of the agonists-WT A_3R complex. Seeking to verify this claim, we mutated V169$^{5.30}$ and the remote I253$^{6.58}$ to glutamate. The functional assays showed a significant activity increase for both agonists for V169$^{5.30}$E, and WT-like activity for I253$^{6.58}$E. The MD simulations for V169$^{5.30}$E A_3R, show that the binding positions for IB-MECA (**3**) and NECA (**2**) are rather stable after 150 ns with RMSD values of 1.83 Å and 1.96 Å, respectively. The interaction plot for IB-MECA (**3**) suggests a very similar binding profile to that of the WT receptor, where the main interactions involve residues T94$^{3.36}$, F168$^{5.29}$, W185$^{5.46}$, W243$^{6.48}$, L246$^{6.51}$, N250$^{6.55}$ and S271$^{7.42}$. Over the course of the trajectories, the agonist moves slightly away from E169$^{5.30}$ and loses its hydrogen bond interactions with H272$^{7.43}$, but the iodobenzyl moiety remains bound towards EL2, TM5 and TM6, establishing frequent hydrophobic contacts with M174$^{5.35}$, M177$^{5.38}$, and I253$^{6.58}$ which are not found to interact directly with agonists in the WT A_3R complex simulations. NECA (**2**) showed a similar movement from its WT binding pose, losing the hydrogen bond interactions with H272$^{7.43}$ and Q167$^{5.28}$ and reducing the van der Waals contacts with W185$^{5.46}$, W243$^{6.48}$ and L246$^{6.51}$. However, NECA (**2**) forms strong hydrogen bond interactions through its 6-NH_2 group with E169$^{5.30}$, as seen in the corresponding crystal structures of A_{2A}R (Figure 8). The MD simulations of IB-MECA (**3**) and NECA (**2**) in complex with I253$^{6.58}$E A_3R also suggest a significant relocation of the agonists due to E253$^{6.58}$, strengthening of the important binding interactions and the formation of new ones due to the plasticity of the binding area, which contribute to a stable complex (SI, Figure S14).

These results support the fact that V169$^{5.30}$ is not the most critical residue for the selectivity of agonists against A_3R, but the selectivity results from the synergy of direct and indirect interactions with lipophilic residues from EL2, TM5 and TM6. Taken together, the results for these mutants suggest that more work needs to be done to discover the role of the lipophilic region in-between EL2, TM5 and TM6 in the subtype-selectivity of agonists like IB-MECA towards A_3R.

(A)

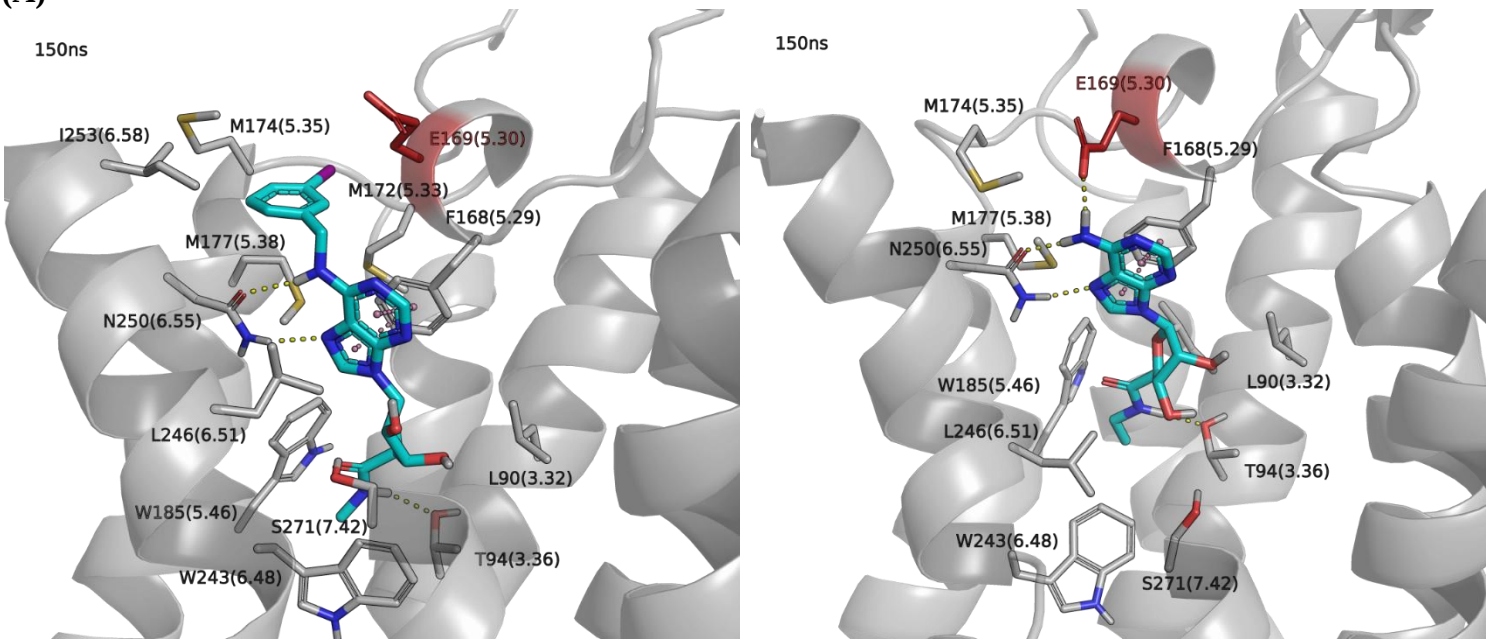
150ns
I253(6.58)
M174(5.35)
E169(5.30)
M172(5.33)
F168(5.29)
M177(5.38)
N250(6.55)
L246(6.51)
L90(3.32)
W185(5.46)
S271(7.42)
T94(3.36)
W243(6.48)
150ns
M174(5.35)
E169(5.30)
F168(5.29)
M177(5.38)
N250(6.55)
W185(5.46)
L90(3.32)
L246(6.51)
T94(3.36)
W243(6.48)
S271(7.42)

(B)

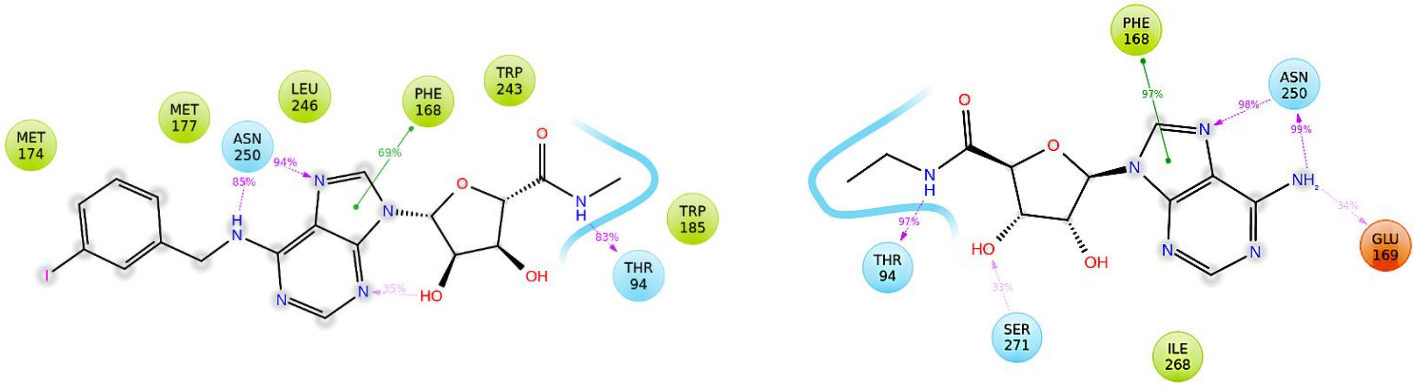
MET 174
MET 177
LEU 246
ASN 250
PHE 168
TRP 243
TRP 185
THR 94
PHE 168
ASN 250
GLU 169
THR 94
SER 271
ILE 268

(C)

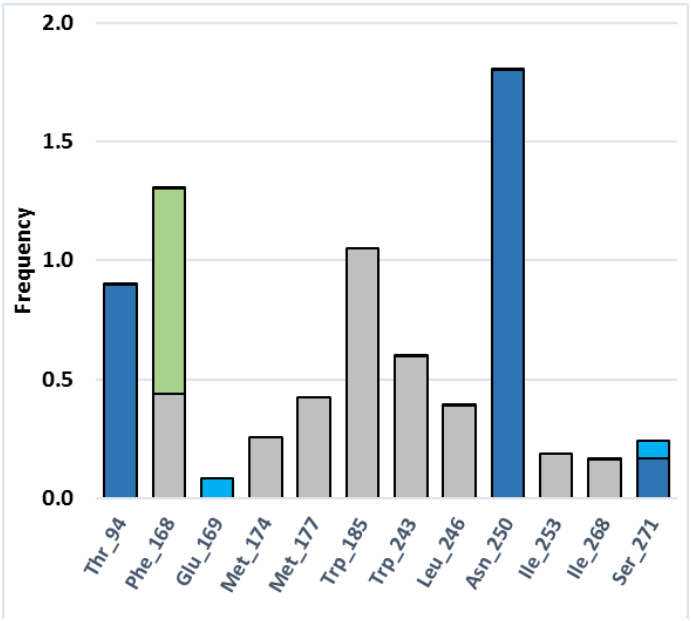
Frequency
2.0
1.5
1.0
0.5
0.0
Thr_94
Phe_168
Glu_169
Met_174
Met_177
Trp_185
Trp_243
Leu_246
Asn_250
Ile_253
Ile_268
Ser_271

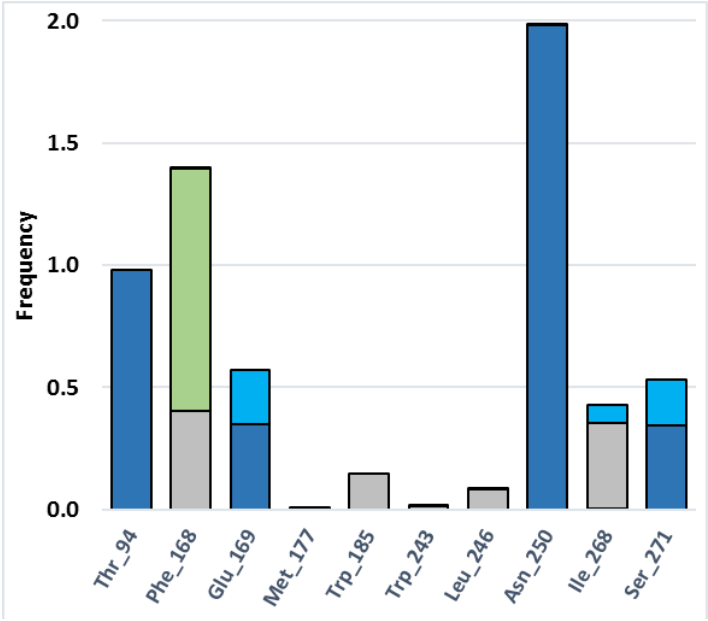
Frequency
2.0
1.5
1.0
0.5
0.0
Thr_94
Phe_168
Glu_169
Met_177
Trp_185
Trp_243
Leu_246
Asn_250
Ile_268
Ser_271

Figure 8. (A) Snapshot of IB-MECA (**3**) (left) and NECA (**2**) (right) inside the V169$^{5.30}$E A_3R binding site at 150 ns of MD simulation, (B) 2D interaction diagram, and (C) receptor-ligand interaction histogram for IB-MECA (left) and NECA (right) inside V169$^{5.30}$E A_3R orthosteric binding area, recorded from 0-150 ns of MD simulation trajectory. Color scheme (A): Ligand=cyan sticks, receptor=white ribbon and sticks, H-bond interactions=yellow dashes, π-π interactions=pink dashes; Color scheme (B): polar surface/residues=blue, hydrophobic residues=green; Color scheme (C): H-bond interactions=dark blue, hydrophobic interactions=grey, π-π interactions=green, water-mediated interactions=light blue. Mutation in shown with a red color in the ribbon of TM5.

5 Conclusions

Binding and activation of GPCRs is a complicated phenomenon. In this study we explored how the activity of a receptor can be related to binding interactions with an orthosteric ligand using a combination of mutagenesis and biomolecular simulations. The study focused on A_3R, whereby the structure has not been experimentally determined yet, and thus we aimed to provide useful information for agonist - orthosteric binding interactions and characterization of the orthosteric binding area.

Of the mutated residues that were found to be in direct contact with the agonists in the WT receptor, the majority, i.e. T94$^{3.36}$A, F168$^{5.29}$A, L246$^{6.51}$A, N250$^{6.55}$A, I268$^{7.39}$A, S271$^{7.42}$A and H272$^{7.43}$A, were found to negate agonist activity. The mutations W185$^{5.46}$A and L264$^{7.35}$A did not affect agonist activity, while V169$^{5.30}$A was found to increase the potency of IB-MECA **(3)** when mutated to alanine and, more notably, increase the potency of both agonists when mutated to glutamic acid.

Mutated residues not in contact with either of the agonists had mixed effects on their potency; negation of activity for both agonists (L90$^{3.32}$A and M177$^{5.38}$A), decreased activity of NECA (**2**) and increased activity of IB-MECA (**3**) (M174$^{5.35}$A), increased activity of NECA (**2**) (I249$^{6.54}$A) or did not affect both agonists activity (I253$^{6.58}$A).

We found that when a hydrophobic residue is replaced with the smaller alanine, various water-mediated interactions appear between the ligand hydrogen bond donor/acceptor atoms and the side or main chain groups of various binding site residues. These contacts usually weaken ligand binding, but in some cases enhance the activity, like for IB-MECA (**3**) - V169$^{5.30}$A A_3R where the agonist translocates and forms direct interactions with S73$^{2.65}$ which is on the edge of the binding site in the WT A_3R.

The above mentioned results from mutagenesis were in fair agreement to the biomolecular simulations results. The calculated ΔG_{eff} values for both IB-MECA (**3**) and NECA (**2**) displayed good correlations with the experimentally determined pIC_{50} values, with r = -0.69 and r = -0.76 respectively (Figure 4). Thus, based on the MM-GBSA calculated ΔG_{eff} values, it is possible to distinguish two sets of mutant receptors, i.e. those that reduce or negate NECA **(2)** or IB-MECA **(3)** activity towards A_3R, or those that bind stably compared to WT A_3R.

In many cases, simple inspection of the trajectories was enough to account for the instability of the complexes, where the average ligand RMSD was in the range 3.8-5.7 Å and many of the stabilizing interactions were lost. However, some mutations that reduce or negate agonist activity, i.e. M177$^{5.38}$A, L90$^{3.32}$A or H272$^{7.43}$A induced conformational changes in the binding area that surprisingly did not affect the agonist position, leading to ligand RMSD values in the range 2.7-3.5 Å. In these cases, the calculation of $\Delta\Delta G_{eff}$, which was over +22 kcal mol^{-1}, was needed to account for the reduction in activity. In the cases of NECA (**2**) - I249$^{6.54}$A A_3R and IB-MECA (**3**) - I253$^{6.58}$E A_3R, the ligand shows a significant translocation from its starting position inside the binding area, with RMSD of ca 3.9 Å and 4.2 Å respectively. However, the agonist - A_3R complex was stabilized since the ligand forms new favorable interactions.

Our results indicate that the π-π interactions with F168$^{5.29}$ and the van der Waals interactions with L246$^{6.51}$ and I268$^{7.39}$ are mandatory for ligand binding and/or receptor activation. Similarly, the activation of A_3R is mediated by the formation of hydrogen bond interactions with T94$^{3.36}$, N250$^{6.55}$ and S271$^{7.42}$. Residue H272$^{7.43}$ was also found to be important for the activity of ligand, but not for ligand binding, according to our computational results.

The experimental and computational results have provided evidence that V169$^{5.30}$ is not crucial for IB-MECA **(3)** selectivity against A_3R, since both its mutation to alanine and -more stunningly- to glutamic acid showed no effect and increased the activity of the agonist, respectively. This finding, along with the fact that other residues of EL2, TM5 and TM6 which are remote from the surface of the binding area, such as L90$^{3.32}$ and M177$^{5.38}$, may act by modulating the structure of the pocket, can have significant impact on the design of potent and selective ligands targeting A_3R. Nevertheless, the significance of these residues and the selectivity mechanism that takes place during the binding of agonists and possibly antagonists inside A_3R needs further investigation.

6 Supporting Information available

Supplementary material includes three Tables and 14 Figures; one Table with cAMP accumulation assay parameters; one Table with MM-GBSA-calculated ΔG_{eff} values; one Table with force field results evaluation; one Figure including to the dose-inhibition curves; two Figures with MM-GBSA-calculated free energies and relative free energies of binding bar charts; 11 Figures describing interaction diagrams, RMSD polts and snapshots for different mutant A_3R - agonist complexes. Also desciption of the results from the MD simulations of agonist - mutant A_3R complexes.

7 Acknowledgements

This research represents part of the Master thesis of DS. and post-doctoral work EV We also thank Chiesi Hellas which supported this research (SARG No 10354) and the State Scholarships Foundation (IKY) for providing a Ph.D fellowship to P.L. (MIS 5000432, NSRF 2014-2020) and a post-doctoral fellowship to E.V. (MIS 5001552, NSRF 2014-2020). We gratefully acknowledge the support of the Leverhulme Trust (KB and GL) and the BBSRC (GL).
This work was supported by computational time granted from the Greek Research & Technology Network (GRNET) in the National HPC facility - ARIS - under project IDs pr002021 and pr001004).

8 Author Information

Address for correspondence. Dr Antonios Kolocouris, Department of Medicinal Chemistry, Faculty of Pharmacy, National and Kapodistrian University of Athens, Panepistimioupolis Zografou, Athens, 15 771. Tel: 210-727-4834, Email: ankol@pharm.uoa.gr.
Dr Graham Ladds, Department of Pharmacology, University of Cambridge, Tennis Court Road, Cambridge, CB2 1PD Tel; +44 (0) 1223 334020. Email: grl30@cam.ac.uk.

Author Contributions. AK and GL conceived and designed the research; KB performed the mammalian assays; DS and PL performed the MD simulations; KB, GL, DS, and AK analyzed the data; DS and AK wrote the manuscript (EV wrote the introduction); KB and GL revised and edited the manuscript.
DS, PL, KB contributed equally.

9 Abbreviations

CNS, central nervous system; Extracellular loop, EL2; FEP, Free Energy Perturbation; GB, Generalized-Born; PDB, GPCRs, G-protein coupled receptors; HEMADO, 2-hexyn-1-yl-N^6-methyladenosine; IB-MECA, 1-deoxy-1-[6-[[(3-iodophenyl)methyl]amino]-9*H*-purin-9-yl]-*N*-methyl-β-D-ribofuranuronamide; MD, Molecular dynamics; NECA, 5'-N-ethylcarboxamidoadenosine; OPM, Orientations of Proteins in Membranes; PD, Parkinson's disease; PDB, Protein data bank; PME, particle mesh Ewald method; POPE, 1-palmitoyl-2-oleoyl-*sn*-glycero-3-phosphoethanolamine; RESPA, Reversible multiple time scale molecular dynamics; RMSD, root-mean-square deviation; Transmembrane, TM

10 References

(1) Fredholm, B. B.; IJzerman, A. P.; Jacobson, K. A.; Klotz, K.-N.; Linden, J. International Union of Pharmacology. XXV. Nomenclature and Classification of Adenosine Receptors. *Pharmacol. Rev.* **2001**, *53*, 527–552.

(2) Fredholm, B. B.; IJzerman, A. P.; Jacobson, K. A.; Linden, J.; Müller, C. E. International Union of Basic and Clinical Pharmacology. LXXXI. Nomenclature and Classification of Adenosine Receptors—an Update. *Pharmacol. Rev.* **2011**, pr--110.

(3) Daly, J. W. Adenosine Receptors: Targets for Future Drugs. *J. Med. Chem.* **1982**.

(4) Chen, J.-F.; Eltzschig, H. K.; Fredholm, B. B. Adenosine Receptors as Drug Targets—What Are the Challenges? *Nat. Rev. Drug Discov.* **2013**, *12*, 265.

(5) Fredholm, B. B. Adenosine Receptors as Drug Targets. *Experimental Cell Research*, 2010.

(6) Gessi, S.; Varani, K.; Merighi, S.; Morelli, A.; Ferrari, D.; Leung, E.; Baraldi, P. G.; Spalluto, G.; Borea, P. A. Pharmacological and Biochemical Characterization of A3 Adenosine Receptors in Jurkat T Cells. *Br. J. Pharmacol.* **2001**, *134*, 116–126.

(7) Madi, L.; Ochaion, A.; Rath-Wolfson, L.; Bar-Yehuda, S.; Erlanger, A.; Ohana, G.; Harish, A.; Merimski, O.; Barer, F.; Fishman, P. The A3 Adenosine Receptor Is Highly Expressed in Tumor versus Normal Cells: Potential Target for Tumor Growth Inhibition. *Clin. Cancer Res.* **2004**, *10*, 4472–4479.

(8) Borea, P. A.; Varani, K.; Vincenzi, F.; Baraldi, P. G.; Tabrizi, M. A.; Merighi, S.; Gessi, S. The A3 Adenosine Receptor: History and Perspectives. *Pharmacol. Rev.* **2015**, *67*, 74–102.

(9) Yao, Y.; Sei, Y.; Abbracchio, M. P.; Jiang, J.-L.; Kim, Y.-C.; Jacobson, K. A. Adenosine A3 Receptor Agonists Protect HL-60 and U-937 Cells from Apoptosis Induced by A3

Antagonists. *Biochem. Biophys. Res. Commun.* **1997**, *232*, 317.

(10) Trincavelli, M. L.; Tuscano, D.; Marroni, M.; Falleni, A.; Gremigni, V.; Ceruti, S.; Abbracchio, M. P.; Jacobson, K. A.; Cattabeni, F.; Martini, C. A3 Adenosine Receptors in Human Astrocytoma Cells: Agonist-Mediated Desensitization, Internalization, and down-Regulation. *Mol. Pharmacol.* **2002**, *62*, 1373–1384.

(11) Merighi, S.; Varani, K.; Gessi, S.; Cattabriga, E.; Iannotta, V.; Ulouglu, C.; Leung, E.; Borea, P. A. Pharmacological and Biochemical Characterization of Adenosine Receptors in the Human Malignant Melanoma A375 Cell Line. *Br. J. Pharmacol.* **2001**, *134*, 1215–1226.

(12) Suh, B.-C.; Kim, T.-D.; Lee, J.-U.; Seong, J.-K.; Kim, K.-T. Pharmacological Characterization of Adenosine Receptors in PGT-β Mouse Pineal Gland Tumour Cells. *Br. J. Pharmacol.* **2001**, *134*, 132–142.

(13) Morello, S.; Petrella, A.; Festa, M.; Popolo, A.; Monaco, M.; Vuttariello, E.; Chiappetta, G.; Parente, L.; Pinto, A. Cl-IB-MECA Inhibits Human Thyroid Cancer Cell Proliferation Independently of A3 Adenosine Receptor Activation. *Cancer Biol. Ther.* **2008**, *7*, 278–284.

(14) Kim, H. O.; Ji, X.; Siddiqi, S. M.; Olah, M. E.; Stiles, G. L.; Jacobson, K. A. 2-Substitution of N6-Benzyladenosine-5'-Uronamides Enhances Selectivity for A3 Adenosine Receptors. *J. Med. Chem.* **1994**, *37*, 3614–3621.

(15) Layland, J.; Carrick, D.; Lee, M.; Oldroyd, K.; Berry, C. Adenosine: Physiology, Pharmacology, and Clinical Applications. *JACC Cardiovasc. Interv.* **2014**, *7*, 581–591.

(16) Volpini, R.; Costanzi, S.; Lambertucci, C.; Taffi, S.; Vittori, S.; Klotz, K.-N.; Cristalli, G. N 6-Alkyl-2-Alkynyl Derivatives of Adenosine as Potent and Selective Agonists at the Human Adenosine A3 Receptor and a Starting Point for Searching A2B Ligands. *J. Med. Chem.* **2002**, *45*, 3271–3279.

(17) Deninno, M. P.; Masamune, H.; Chenard, L. K.; DiRico, K. J.; Eller, C.; Etienne, J. B.; Tickner, J. E.; Kennedy, S. P.; Knight, D. R.; Kong, J. 3 '-Aminoadenosine-5 '-Uronamides: Discovery of the First Highly Selective Agonist at the Human Adenosine A3 Receptor. *J. Med. Chem.* **2003**, *46*, 353–355.

(18) Jeong, L. S.; Jin, D. Z.; Kim, H. O.; Shin, D. H.; Moon, H. R.; Gunaga, P.; Chun, M. W.; Kim, Y.-C.; Melman, N.; Gao, Z.-G. N6-Substituted D-4 '-Thioadenosine-5 '-Methyluronamides: Potent and Selective Agonists at the Human A3 Adenosine Receptor. *J. Med. Chem.* **2003**, *46*, 3775–3777.

(19) Tchilibon, S.; Joshi, B. V; Kim, S.-K.; Duong, H. T.; Gao, Z.-G.; Jacobson, K. A. (N)-Methanocarba 2, N 6-Disubstituted Adenine Nucleosides as Highly Potent and Selective A3 Adenosine Receptor Agonists. *J. Med. Chem.* **2005**, *48*, 1745–1758.

(20) Melman, A.; Wang, B.; Joshi, B. V; Gao, Z.-G.; de Castro, S.; Heller, C. L.; Kim, S.-K.;

Jeong, L. S.; Jacobson, K. A. Selective A3 Adenosine Receptor Antagonists Derived from Nucleosides Containing a Bicyclo [3.1. 0] Hexane Ring System. *Bioorg. Med. Chem.* **2008**, *16*, 8546–8556.

(21) Fishman, P.; Bar-Yehuda, S.; Liang, B. T.; Jacobson, K. A. Pharmacological and Therapeutic Effects of A3 Adenosine Receptor Agonists. *Drug Discov. Today* **2012**, *17*, 359–366.

(22) Jacobson, K. A.; Tosh, D. K.; Jain, S.; Gao, Z.-G. Historical and Current Adenosine Receptor Agonists in Preclinical and Clinical Development. *Front. Cell. Neurosci.* **2019**, *13*, 1–17.

(23) Salvatore, C. A.; Tilley, S. L.; Latour, A. M.; Fletcher, D. S.; Koller, B. H.; Jacobson, M. A. Disruption of the A3 Adenosine Receptor Gene in Mice and Its Effect on Stimulated Inflammatory Cells. *J. Biol. Chem.* **2000**.

(24) Kreckler, L. M. Adenosine Inhibits Tumor Necrosis Factor- Release from Mouse Peritoneal Macrophages via A2A and A2B but Not the A3 Adenosine Receptor. *J. Pharmacol. Exp. Ther.* **2006**.

(25) Blackburn, M. R.; Vance, C. O.; Morschl, E.; Wilson, C. N. Adenosine Receptors and Inflammation. In *Adenosine receptors in health and disease*; Springer, 2009; pp. 215–269.

(26) Lebon, G.; Warne, T.; Edwards, P. C.; Bennett, K.; Langmead, C. J.; Leslie, A. G. W.; Tate, C. G. Agonist-Bound Adenosine A2A Receptor Structures Reveal Common Features of GPCR Activation. *Nature* **2011**, *474*, 521.

(27) Xu, F.; Wu, H.; Katritch, V.; Han, G. W.; Jacobson, K. A.; Gao, Z.-G.; Cherezov, V.; Stevens, R. C. Structure of an Agonist-Bound Human A2A Adenosine Receptor. *Science (80-.).* **2011**, *332*, 322–327.

(28) White, K. L.; Eddy, M. T.; Gao, Z.-G.; Han, G. W.; Lian, T.; Deary, A.; Patel, N.; Jacobson, K. A.; Katritch, V.; Stevens, R. C. Structural Connection between Activation Microswitch and Allosteric Sodium Site in GPCR Signaling. *Structure* **2018**, *26*, 259--269.e5.

(29) Jaakola, V.-P.; Griffith, M. T.; Hanson, M. A.; Cherezov, V.; Chien, E. Y. T.; Lane, J. R.; IJzerman, A. P.; Stevens, R. C. The 2.6 Angstrom Crystal Structure of a Human A2A Adenosine Receptor Bound to an Antagonist. *Science (80-.).* **2008**, *322*, 1211–1217.

(30) Congreve, M.; Andrews, S. P.; Doré, A. S.; Hollenstein, K.; Hurrell, E.; Langmead, C. J.; Mason, J. S.; Ng, I. W.; Tehan, B.; Zhukov, A.; Weir, M.; Marshall, F. H. Discovery of 1,2,4-Triazine Derivatives as Adenosine A2A Antagonists Using Structure Based Drug Design. *J. Med. Chem.* **2012**, *55*, 1898–1903.

(31) Sun, B.; Bachhawat, P.; Chu, M. L.-H.; Wood, M.; Ceska, T.; Sands, Z. A.; Mercier, J.; Lebon, F.; Kobilka, T. S.; Kobilka, B. K. Crystal Structure of the Adenosine A2A Receptor Bound to an Antagonist Reveals a Potential Allosteric Pocket. *Proc. Natl. Acad. Sci.* **2017**, *114*, 2066–2071.

(32) Liu, W.; Chun, E.; Thompson, A. A.; Chubukov, P.; Xu, F.; Katritch, V.; Han, G. W.; Roth, C. B.; Heitman, L. H.; IJzerman, A. P.; Cherezov, V.; Stevens, R. C. Structural Basis for Allosteric Regulation of GPCRs by Sodium Ions. *Science (80-.).* **2012**, *337*, 232–236.

(33) Doré, A. S.; Robertson, N.; Errey, J. C.; Ng, I.; Hollenstein, K.; Tehan, B.; Hurrell, E.; Bennett, K.; Congreve, M.; Magnani, F.; Tate, C. G.; Weir, M.; Marshall, F. H. Structure of the Adenosine A2A Receptor in Complex with ZM241385 and the Xanthines XAC and Caffeine. *Structure* **2011**, *19*, 1283–1293.

(34) Cheng, R. K. Y.; Segala, E.; Robertson, N.; Deflorian, F.; Doré, A. S.; Errey, J. C.; Fiez-Vandal, C.; Marshall, F. H.; Cooke, R. M. Structures of Human A1 and A2A Adenosine Receptors with Xanthines Reveal Determinants of Selectivity. *Structure* **2017**, *25*, 1275-1285.e4.

(35) Glukhova, A.; Thal, D. M.; Nguyen, A. T.; Vecchio, E. A.; Jörg, M.; Scammells, P. J.; May, L. T.; Sexton, P. M.; Christopoulos, A. Structure of the Adenosine A1 Receptor Reveals the Basis for Subtype Selectivity. *Cell* **2017**, *168*, 867--877.e13.

(36) Draper-Joyce, C. J.; Khoshouei, M.; Thal, D. M.; Liang, Y.-L.; Nguyen, A. T. N.; Furness, S. G. B.; Venugopal, H.; Baltos, J.-A.; Plitzko, J. M.; Danev, R.; Baumeister, W.; May, L. T.; Wootten, D.; Sexton, P. M.; Glukhova, A.; Christopoulos, A. Structure of the Adenosine-Bound Human Adenosine A1 Receptor-Gi Complex. *Nature* **2018**.

(37) Gao, Z.-G.; Chen, A.; Barak, D.; Kim, S.-K.; Müller, C. E.; Jacobson, K. A. Identification by Site-Directed Mutagenesis of Residues Involved in Ligand Recognition and Activation of the Human A3 Adenosine Receptor. *J. Biol. Chem.* **2002**, *277*, 19056–19063.

(38) Gao, Z.-G.; Kim, S.-K.; Biadatti, T.; Chen, W.; Lee, K.; Barak, D.; Kim, S. G.; Johnson, C. R.; Jacobson, K. A. Structural Determinants of A3 Adenosine Receptor Activation: Nucleoside Ligands at the Agonist/Antagonist Boundary. *J. Med. Chem.* **2002**, *45*, 4471–4484.

(39) Gao, Z.-G.; Kim, S.-K.; Gross, A. S.; Chen, A.; Blaustein, J. B.; Jacobson, K. A. Identification of Essential Residues Involved in the Allosteric Modulation of the Human A3 Adenosine Receptor. *Mol. Pharmacol.* **2003**, *63*, 1021–1031.

(40) Nguyen, A. T. N.; Vecchio, E. A.; Thomas, T.; Nguyen, T. D.; Chemist, A.; Scammels, P. J.; White, P. J.; Sexton, P. M.; Gregory, K. J.; May, L. T.; Christopoulos, A. The Role of the Second Extracellular Loop of the Adenosine A1 Receptor on Allosteric Modulator Binding, Signaling and Cooperativity. *Mol. Pharmacol.* **2016**.

(41) Keränen, H.; Gutiérrez-de-Terán, H.; Åqvist, J. Structural and Energetic Effects of A2A Adenosine Receptor Mutations on Agonist and Antagonist Binding. *PLoS One* **2014**.

(42) Keränen, H.; Åqvist, J.; Gutiérrez-De-Terán, H. Free Energy Calculations of A2Aadenosine

Receptor Mutation Effects on Agonist Binding. *Chem. Commun.* **2015**.

(43) Matricon, P.; Ranganathan, A.; Warnick, E.; Gao, Z.-G.; Rudling, A.; Lambertucci, C.; Marucci, G.; Ezzati, A.; Jaiteh, M.; Dal Ben, D.; Jacobson, K. A.; Carlsson, J. Fragment Optimization for GPCRs by Molecular Dynamics Free Energy Calculations: Probing Druggable Subpockets of the A 2A Adenosine Receptor Binding Site. *Sci. Rep.* **2017**, *7*, 6398.

(44) Pan, A. C.; Borhani, D. W.; Dror, R. O.; Shaw, D. E. Molecular Determinants of Drug-Receptor Binding Kinetics. *Drug Discov. Today* **2013**, *18*, 667–673.

(45) Jaakola, V. P.; Griffith, M. T.; Hanson, M. A.; Cherezov, V.; Chien, E. Y. T.; Lane, J. R.; Ijzerman, A. P.; Stevens, R. C. The 2.6 Angstrom Crystal Structure of a Human A2Aadenosine Receptor Bound to an Antagonist. *Science (80-.).* **2008**, *322*, 1211–1217.

(46) Lagarias, P.; Vrontaki, E.; Lambrinidis, G.; Stamatis, D.; Convertino, M.; Ortore, G.; Mavromoustakos, T.; Klotz, K.-N.; Kolocouris, A. Discovery of Novel Adenosine Receptor Antagonists through a Combined Structure-and Ligand-Based Approach Followed by Molecular Dynamics Investigation of Ligand Binding Mode. *J. Chem. Inf. Model.* **2018**, *58*, 794–815.

(47) Homeyer, N.; Stoll, F.; Hillisch, A.; Gohlke, H. Binding Free Energy Calculations for Lead Optimization: Assessment of Their Accuracy in an Industrial Drug Design Context. *J. Chem. Theory Comput.* **2014**, *10*, 3331–3344.

(48) Floris, M.; Sabbadin, D.; Medda, R.; Bulfone, A.; Moro, S. Adenosiland: Walking through Adenosine Receptors Landscape. *Eur. J. Med. Chem.* **2012**, *58*, 248–257.

(49) Ballesteros, J. A.; Weinstein, H. *Receptor Molecular Biology*; 1995; Vol. 25.

(50) Protein Preparation Wizard 2015-2; Epik Version 2.4, Schrödinger, LLC, New York, NY, 2015; Impact Version 5.9, Schrödinger, LLC, New York, NY, 2015; Prime Version 3.2, Schrödinger, LLC, New York, NY, 2015. *Protein Prep. Wizard 2015-2; Epik version 2.4, Schrödinger, LLC, New York, NY, 2015; Impact version 5.9, Schrödinger, LLC, New York, NY, 2015; Prime version 3.2, Schrödinger, LLC, New York, NY, 2015*.

(51) Kaminski, G. A.; Friesner, R. A.; Tirado-Rives, J.; Jorgensen, W. L. Evaluation and Reparametrization of the OPLS-AA Force Field for Proteins via Comparison with Accurate Quantum Chemical Calculations on Peptides. *J. Phys. Chem. B* **2001**, *105*, 6474–6487.

(52) Katritch, V.; Kufareva, I.; Abagyan, R. Structure Based Prediction of Subtype-Selectivity for Adenosine Receptor Antagonists. *Neuropharmacology* **2011**, *60*, 108–115.

(53) GOLD Suite, Version 5.2; Cambridge Crystallographic Data Centre: Cambridge, U.K., 2015. *GOLD Suite, version 5.2; Cambridge Crystallogr. Data Cent. Cambridge, U.K., 2015*.

(54) Jones, G.; Willett, P.; Glen, R. C.; Leach, A. R.; Taylor, R. Development and Validation of a

Genetic Algorithm for Flexible Docking. *J. Mol. Biol.* **1997**, *267*, 727–748.

(55) Verdonk, M. L.; Chessari, G.; Cole, J. C.; Hartshorn, M. J.; Murray, C. W.; Nissink, J. W. M.; Taylor, R. D.; Taylor, R. Modeling Water Molecules in Protein- Ligand Docking Using GOLD. *J. Med. Chem.* **2005**, *48*, 6504–6515.

(56) Eldridge, M. D.; Murray, C. W.; Auton, T. R.; Paolini, G. V; Mee, R. P. Empirical Scoring Functions: I. The Development of a Fast Empirical Scoring Function to Estimate the Binding Affinity of Ligands in Receptor Complexes. *J. Comput. Aided. Mol. Des.* **1997**, *11*, 425–445.

(57) Glide, Schrödinger, LLC, New York, NY, 2012. Glide, Version 5.7. *Glide Schrödinger LLC NY*, 2011.

(58) Jorgensen, W. L.; Maxwell, D. S.; Tirado-Rives, J. Development and Testing of the OPLS All-Atom Force Field on Conformational Energetics and Properties of Organic Liquids. *J. Am. Chem. Soc.* **1996**, *118*, 11225–11236.

(59) Rizzo, R. C.; Jorgensen, W. L. OPLS All-Atom Model for Amines: Resolution of the Amine Hydration Problem. *J. Am. Chem. Soc.* **1999**, *121*, 4827–4836.

(60) Wang, J.; Cieplak, P.; Kollman, P. A. How Well Does a Restrained Electrostatic Potential (RESP) Model Perform in Calculating Conformational Energies of Organic and Biological Molecules? *J. Comput. Chem.* **2000**, *21*, 1049–1074.

(61) Hornak, V.; Abel, R.; Okur, A.; Strockbine, B.; Roitberg, A.; Simmerling, C. Comparison of Multiple Amber Force Fields and Development of Improved Protein Backbone Parameters. *Proteins Struct. Funct. Bioinforma.* **2006**, *65*, 712–725.

(62) Best, R. B.; Zhu, X.; Shim, J.; Lopes, P. E. M.; Mittal, J.; Feig, M.; MacKerell, A. D. Optimization of the Additive CHARMM All-Atom Protein Force Field Targeting Improved Sampling of the Backbone ϕ, ψ and Side-Chain χ_1 and χ_2 Dihedral Angles. *J. Chem. Theory Comput.* **2012**, *8*, 3257–3273.

(63) Desmond Molecular Dynamics System, Version 3.0, D.E. Shaw Research: New York, 2011. *Desmond Mol. Dyn. Syst. version 3.0; D.E. Shaw Res. New York, 2011; Maest. Interoperability Tools, 3.1; Schrodinger Res. New York, 2012*.

(64) Maestro-Desmond Interoperability Tools, Version 3.1; Schrodinger: New York, 2012.

(65) Jorgensen, W. L.; Chandrasekhar, J.; Madura, J. D.; Impey, R. W.; Klein, M. L. Comparison of Simple Potential Functions for Simulating Liquid Water. *J. Chem. Phys.* **1983**, *79*, 926–935.

(66) Wang, J.; Wolf, R. M.; Caldwell, J. W.; Kollman, P. A.; Case, D. A. Development and Testing of a General Amber Force Field. *J. Comput. Chem.* **2004**, *25*, 1157–1174.

(67) Case, D. A.; Babin, V.; Berryman, J. T.; Betz, R. M.; Cai, Q.; Ceruti, D. S.; Cheatam, I. I. I. T. E.; Darden, T. A.; Duke, R. E.; Gohlke, H.; Goetz, A. W.; Gusarov, S.; Homeyer, N.;

Janowski, P.; Kaus, J.; Kolossváry, I.; Kovalenko, A.; Lee, T. S.; LeGrand, S.; Luchko, T.; Luo, R.; Madej, B.; Merz, K. M.; Paesani, F.; Roe, D. R.; Roitberg, A.; Sagui, C.; Salomon-Ferrer, R.; Seabra, G.; Simmerling, C. L.; Smith, W.; Swails, J.; Walker, R. C.; Wang, J.; Wolf, R. M.; Wu, X.; Kollman, P. A. AMBER 14; University of California: San Francisco, CA, 2014.

(68) Darden, T.; York, D.; Pedersen, L. Particle Mesh Ewald: An N·log(N) Method for Ewald Sums in Large Systems. *J. Chem. Phys.* **1993**, *98*, 10089–10092.

(69) Essmann, U.; Perera, L.; Berkowitz, M. L.; Darden, T.; Lee, H.; Pedersen, L. G. A Smooth Particle Mesh Ewald Method. *J. Chem. Phys.* **1995**, *103*, 8577–8593.

(70) Ryckaert, J.-P.; Ciccotti, G.; Berendsen, H. J. . Numerical Integration of the Cartesian Equations of Motion of a System with Constraints: Molecular Dynamics of n-Alkanes. *J. Comput. Phys.* **1977**, *23*, 327–341.

(71) Martyna, G. J.; Klein, M. L.; Tuckerman, M. Nosé–Hoover Chains: The Canonical Ensemble via Continuous Dynamics. *J. Chem. Phys.* **1992**, *97*, 2635–2643.

(72) Martyna, G. J.; Tobias, D. J.; Klein, M. L. Constant Pressure Molecular Dynamics Algorithms. *J. Chem. Phys.* **1994**, *101*, 4177–4189.

(73) Humphreys, D. D.; Friesner, R. a.; Berne, B. J. A Multiple-Time-Step Molecular Dynamics Algorithm for Macromolecules. *J. Phys. Chem.* **1994**, *98*, 6885–6892.

(74) Massova, I.; Kollman, P. A. Combined Molecular Mechanical and Continuum Solvent Approach (MM-PBSA/GBSA) to Predict Ligand Binding. *Perspect. drug Discov. Des.* **2000**, *18*, 113–135.

(75) Gohlke, H.; Case, D. A. Converging Free Energy Estimates: MM-PB(GB)SA Studies on the Protein-Protein Complex Ras-Raf. *J. Comput. Chem.* **2004**, *25*, 238–250.

(76) Li, J.; Abel, R.; Zhu, K.; Cao, Y.; Zhao, S.; Friesner, R. A. The VSGB 2.0 Model: A next Generation Energy Model for High Resolution Protein Structure Modeling. *Proteins Struct. Funct. Bioinforma.* **2011**.

(77) Weston, C.; Poyner, D.; Patel, V.; Dowell, S.; Ladds, G. Investigating G Protein Signalling Bias at the Glucagon-like Peptide-1 Receptor in Yeast. *Br. J. Pharmacol.* **2014**.

(78) Knight, A.; Hemmings, J. L.; Winfield, I.; Leuenberger, M.; Frattini, E.; Frenguelli, B. G.; Dowell, S. J.; Lochner, M.; Ladds, G. Discovery of Novel Adenosine Receptor Agonists That Exhibit Subtype Selectivity. *J. Med. Chem.* **2016**, *59*, 947–964.

(79) Almerico, A. M.; Tutone, M.; Pantano, L.; Lauria, A. A3 Adenosine Receptor: Homology Modeling and 3D-QSAR Studies. *J. Mol. Graph. Model.* **2013**.

(80) Baltos, J.-A.; Paoletta, S.; Nguyen, A. T. N.; Gregory, K. J.; Tosh, D. K.; Christopoulos, A.; Jacobson, K. A.; May, L. T. Structure-Activity Analysis of Biased Agonism at the Human

Adenosine A3 Receptor. *Mol. Pharmacol.* **2016**.

(81) Stoddart, L. A.; Kellam, B.; Briddon, S. J.; Hill, S. J. Effect of a Toggle Switch Mutation in TM6 of the Human Adenosine A 3 Receptor on Gi Protein-Dependent Signalling and Gi-Independent Receptor Internalization. *Br. J. Pharmacol.* **2014**.

(82) Gao, Z.-G.; Duong, H. T.; Sonina, T.; Kim, S.-K.; Van Rompaey, P.; Van Calenbergh, S.; Mamedova, L.; Kim, H. O.; Kim, M. J.; Kim, A. Y.; Liang, B. T.; Jeong, L. S.; Jacobson, K. A. Orthogonal Activation of the Reengineered A3 AdenosineReceptor (Neoceptor) Using Tailored Nucleoside Agonists. *J. Med. Chem.* **2006**, *49*, 2689–2702.

(83) Jacobson, K. A.; Gao, Z.-G.; Chen, A.; Barak, D.; Kim, S.-A.; Lee, K.; Link, A.; Rompaey, P. Van; van Calenbergh, S.; Liang, B. T. Neoceptor Concept Based on Molecular Complementarity in GPCRs: A Mutant Adenosine A3 Receptor with Selectively Enhanced Affinity for Amine-Modified Nucleosides. *J. Med. Chem.* **2001**, *44*, 4125–4136.

(84) Barkan, K.; Lagarias, P.; Vrontaki, E.; Stamatis, D.; Hoare, S.; Klotz, K.-N.; Kolocouris, A.; Ladds, G. Pharmacological Characterisation of Novel Adenosine Receptor A3R Antagonists. Https://Doi.Org/10.1101/693796. 3.

(85) Li, J.; Jonsson, A. L.; Beuming, T.; Shelley, J. C.; Voth, G. A. Ligand-Dependent Activation and Deactivation of the Human Adenosine A 2A Receptor. *J. Am. Chem. Soc.* **2013**.

TOC GRAPHIC

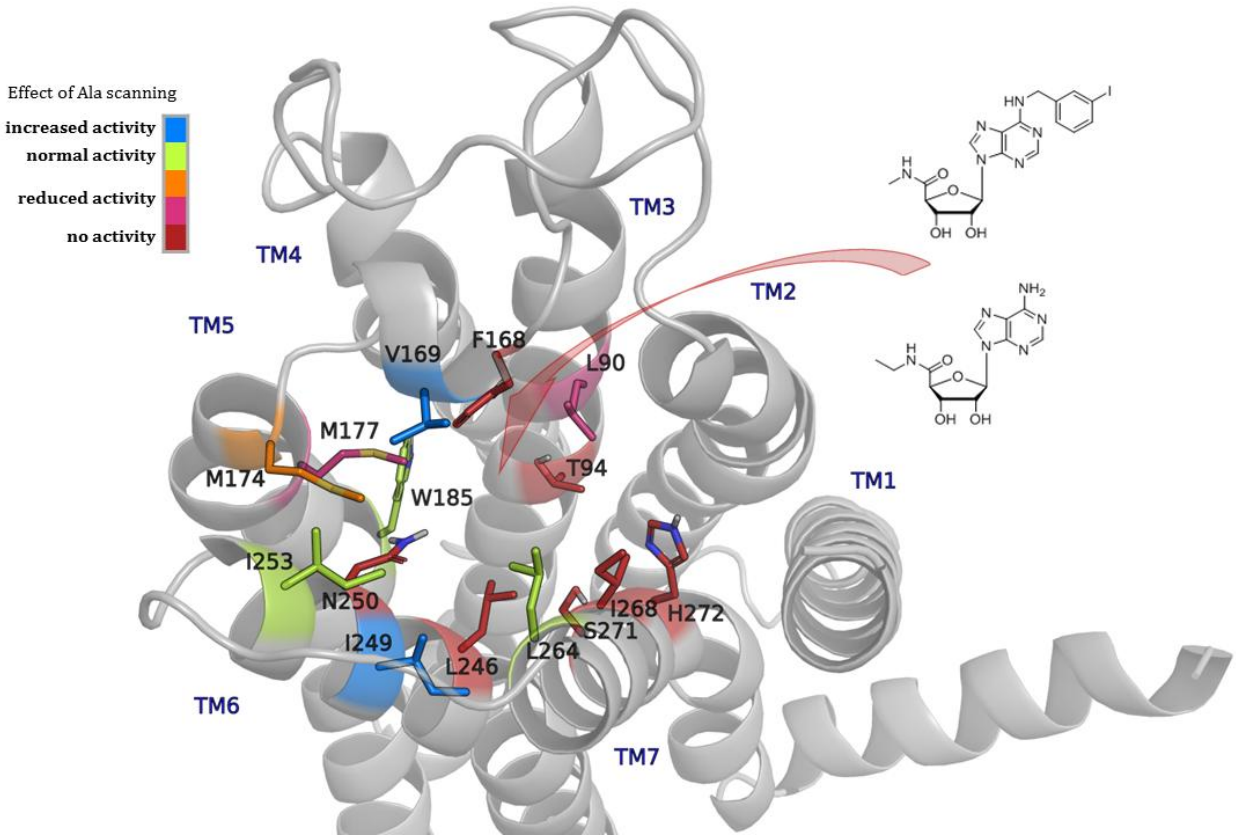
Effect of Ala scanning
increased activity
normal activity
reduced activity
no activity
TM4
TM3
TM2
TM5
TM1
TM6
TM7
V169
F168
L90
M177
M174
W185
T94
I253
N250
I249
L246
L264
I268
H272
S271